MICROWAVE MEASUREMENTS OF DIELECTRIC MATERIAL TO BE USED IN THE CERN FUTURE CIRCULAR COLLIDER STUDY

A Degree Thesis
Submitted to the Faculty of the
Escola Tècnica d'Enginyeria de Telecomunicació de Barcelona
Universitat Politècnica de Catalunya
by
Albert Díez Comas

In partial fulfillment
of the requirements for the degree in
TELECOMMUNICATIONS TECHNOLOGIES
AND SERVICES ENGINEERING

Advisors:
Prof.Dr. Joan M. O'Callaghan
Dra. Montse Pont
M.Sc. Patrick Krkotić

Barcelona, September 2020

Abstract

This thesis is performed in the framework of a project between Universitat Politècnica de Catalunya (UPC), ALBA Synchrotron (ALBA), Institut de Ciència de Materials de Barcelona (ICMAB), Institut de Física d'Altes Energies (IFAE) and Conseil Européen pour la Recherche Nucléaire (CERN), which expects to characterize the surface impedance of high-temperature superconducting coated conductors (HTS-CCs). This material is proposed to be used as coating in the beam screen in the Future Circular Collider (FCC) in order to decrease the resistive wall impedance.

The main objective of this project is to design, fabricate and test a resonator capable of measuring the required properties of different dielectric samples in the microwave region for a temperature range of 20 – 100 K that will be later used to characterize the HTS-CCs. Results for Rutile and Strontium Titanate are presented.

Resum

Aquesta tesi es realitza en el marc d'un projecte entre la Universitat Politècnica de Catalunya (UPC), ALBA Synchrotron (ALBA), l'Institut de Ciència de Materials de Barcelona (ICMAB), l'Institut de Física d'Altes Energies (IFAE) i el Conseil Européen pour la Recherche Nucléaire (CERN), que espera caracteritzar la impedància superficial de conductors recoberts de superconductors d'alta temperatura (HTS-CCs). Aquest material ha estat proposat com a recobriment en la pantalla de feixos del Future Circular Collider (FCC) per tal de disminuir la impedància de la paret resistiva.

L'objectiu principal d'aquest projecte és dissenyar, fabricar i provar un ressonador capaç de mesurar les propietats requerides de diferents mostres dielèctriques en la regió de microones per a un rang de temperatura entre 20 - 100 K que posteriorment s'utilitzarà per caracteritzar els HTS-CCs. Es presenten resultats per al Rútil i Titanat d'Estronci.

Resumen

Esta tesis se realiza en el marco de un proyecto entre la Universitat Politècnica de Catalunya (UPC), ALBA Synchrotron (ALBA), Institut de Ciència de Materials de Barcelona (ICMAB), Institut de Física d'Altes Energies (IFAE) y Conseil Européen pour la Recherche Nucléaire (CERN), que espera caracterizar la impedancia superficial de conductores recubiertos de superconductores de alta temperatura (HTS-CCs). Este material ha sido propuesto para que se utilice como revestimiento en la pantalla de haz en el Future Circular Collider (FCC) para disminuir la impedancia de la pared resistiva.

El objetivo principal de este proyecto es diseñar, fabricar y probar un resonador capaz de medir las propiedades requeridas de diferentes muestras dieléctricas en la región de microondas para un rango de temperatura entre 20 - 100 K que luego se utilizará para caracterizar los HTS-CCs. Se presentan resultados para el Rutilo y Titanato de Estroncio.

Acknowledgements

I wish to express my sincere gratitude to Dr. Joan O'Callaghan, professor at UPC and my tutor, for giving me the opportunity to embark on this project, for his endless help, guidance and insight throughout this research project.

I would also like to thank Dra. Montse Pont, head of Operations Coordination Office at ALBA, for giving me the opportunity to stay in ALBA and the support given during these weeks.

My sincere thanks goes to Patrick Krkotić, PhD student at ALBA and UPC, for always encouraging me, for his patience and enthusiasm. His support helped me in all the time of research and writing of this thesis.

Last but not least, I would like to thank my family, for their caring and for supporting me throughout my life.

Revision history and approval record

Revision	Date	Purpose
0	23/06/2020	Document creation
1	30/06/2020	Structure revision
2	14/07/2020	First document revision
3	28/07/2020	Second document revision
4	11/08/2020	Third document revision
5	24/08/2020	Document upload

DOCUMENT DISTRIBUTION LIST

Name	e-mail
Albert Díez	albertdiezcomas@gmail.com
Joan M. O'Callaghan	joano@tsc.upc.edu
Montse Pont	pont@cells.es
Patrick Krkotić	pkrkotic@cells.es

Written by:		Reviewed and approved by:	
Date	24/08/2020	Date	24/08/2020
Name	Albert Díez	Name	Joan M. O'Callaghan Montse Pont Patrick Krkotić
Position	Project Author	Position	Project Supervisor

Table of contents

Abstract 3

Resum 5

Resumen 7

Acknowledgements 9

Revision history and approval record 11

Table of contents 13

List of Figures 15

List of Tables: 17

1. Introduction 19

1.1. Statement of purpose 19

1.2. Methods, procedures and software 20

1.3. Work plan 22

1.4. Incidences 23

2. Resonator basics 25

2.1. Fundamentals 25

2.2. Quality factor (Q) 25

2.3. Calculating resonator losses 26

2.3.1. Dielectric losses 27

2.3.2. Conductor losses 28

2.4. Coupling factors for two-ports resonators 29

2.4.1. S-Parameters 29

2.4.2. Coupling coefficients 30
3. Simulations 33
3.1. CST Studio Suite software 33
3.1.1. Eigenmode Solver 33
3.1.2. Frequency Domain Solver 35
3.2. Definitions of $TE_{01\delta}$ and $TM_{01\delta}$ modes 36
3.3. Computation of relative loss distribution for cavity design 38
3.4. Computation of geometric and filling factors with CST simulations 42
4. Tests in the laboratory and results 47
4.1. Test at room temperature 47
4.2. Measurement procedure 48
4.3. Measurement of surface resistance vs. temperature 49
4.4. Measurement of Rutile vs. temperature 52
4.5. Measurement of Strontium Titanate vs. temperature 56
5. Budget 59
6. Summary, conclusions and outlook 61
Appendices A: 63
Glossary 65
Bibliography: 67

List of Figures

1.1. Internal diagram of dielectric resonator 21

1.2. Measurement setup 22

1.3. Project Gantt chart 23

2.1. Anisotropic dielectric-loaded parallel plate waveguide 28

2.2. Power waves of a two-port device under test 30

2.3. S-Parameters of a two-port device under test 31

3.1. Mesh view of the dielectric resonator 34

3.2. Cross section of transversal plane of resonator 34

3.3. Cross section of frontal plane of resonator 34

3.4. External view of full model of resonator 35

3.5. Cross section of transversal plane of full model resonator 35

3.6. Cross section of frontal plane of full model resonator 36

3.7. CST simulations of e-field of TE-mode 39

3.8. CST simulations of h-field of TM-mode 40

3.9. Dielectric resonator dimensions 42

4.1. PTFE properties in function of temperature 48

4.2. Resonator mounted in cryogenic refrigerator 49

4.3. Surface resistance of empty cavity 51

4.4. Resonant frequency of empty cavity 51

4.5. Resistivity of empty cavity 52

4.6. Resonant frequency for Rutile 54
4.7. Permittivity of Rutile 55
4.8. Loss tangent of Rutile 55
4.9. Resonant frequency for Strontium Titanate 57
4.10. Permittivity of Strontium Titanate 57
4.11. Loss tangent of Strontium Titanate 58
4.12. Strontium Titanate properties 58

List of Tables:

1.1. Project milestones 23

3.1. Parameters of dielectrics for simulation 41

3.2. Simulated parameters of empty cavity at room temperature 45

3.3. Simulated parameters of dielectric resonator at room temperature 46

3.4. Simulated parameters of empty cavity at 50 K 46

3.5. Simulated parameters of dielectric resonator at 50 K 46

1. Introduction

1.1. Statement of purpose

The Future Circular Collider Study (FCC) [1], hosted by CERN, is developing designs for particle colliders, which seek to extend the research advancements currently obtained at the Large Hadron Collider (LHC). The study is an international collaboration of more than 150 universities, research institutes and industrial partners from all over the world. The FCC examines scenarios for three different types of particle collisions: proton-proton collisions, electron-positron collisions, and proton-electron collisions. In January 2019, a conceptual design report [2]-[5] was submitted as input to the next update of the European Strategy for Particle Physics.

Every particle accelerator consists of a cylindrical-like metallic pipe, usually called beam pipe, in which the particles circulate within it. These charged particles induce an image current in the inner part of the beam pipe, leading to instabilities for the circulating particles. Main factor of this instability is the surface impedance of the material used to construct the beam pipe and the resulting losses are called resistive wall impedance. Therefore, a good conducting material as copper with $RRR = 100$ is desired for the coating of the inner part of the beam pipe of the FCC proton-proton version.

Anyhow, in order to decrease the resistive wall impedance and with that increase the stability of the beam, it is proposed to coat the beam pipe with high-temperature superconducting coated conductors (HTS-CCs). For this reason, an investigation to obtain the properties of this superconducting material at FCC proton-proton conditions is under study. The surface impedance of these HTS coated conductors is measured using a dielectric cavity which is closed by the samples to be examined. Hereby, between the samples, a dielectric puck, with high permittivity and low losses, is put within a cylindrical resonator to measure at moderate frequencies. The

resonator is placed within a 9 T magnet, and the S-Parameters are extracted using a vector network analyzer (VNA) for a range of temperature between 20 K and 100 K.

In order to be able to determine the surface impedance correctly, it is necessary to know the properties of the dielectrics used. The surface resistance is calculated from the resulting quality factor which depends strongly on the loss tangent of the dielectric used. The surface reactance depends on changes in frequencies and therefore the knowledge of the permittivity is mandatory. Due to this, the main objective of the underlying work is the design and construction of a measurement device to determine the dielectric properties of selected dielectric materials in the temperature range between 20 and 100 K. Nevertheless, the study includes an extension of the temperature range until room temperature to be able to broaden the possibilities of measurements of other materials in the future.

1.2. Methods, procedures and software

To measure the main parameters of the dielectric, a well established technique by J.Breeze [6] was adapted to our purposes. The technique uses a shielded dielectric resonator, see Fig. 1.1, mounted in a cryogenic closed-cycle refrigerator which is able to decrease the temperature to 10 K. The already existing dielectric samples have a cylindrical form, and are maintained in the middle of the resonator by two PTFE rods to reduce conductive losses. The coupling of the microwave energy is accomplished by loops attached to the sides of the cavity. The orientation of the loops normal to cylindrical cavity axis excites the TE_{0nm} modes or if rotated 90º they excite the TM_{0nm} modes.

The system needs to work in vacuum for low heat transfer at cryogenic temperatures. At these low pressures, the gas molecules are so far apart that convection is virtually eliminated. Furthermore, it is necessary in order to avoid any crystallization of molecules of the atmosphere. The vacuum is accomplished with a compact vacuum pump system, see Fig. 1.2. Resonant frequencies and quality factors of the resonator are measured at discrete temperature intervals using a vector network analyzer. The dielectric properties are extracted by performing simulations in the numerical simulation software; Computer Simulation Technology (CST) [7] to determine the necessary parameters to extract the loss tangent and permittivity.

The dielectric resonator was designed according to the simulations in CST. A study of different cavity sizes using three different dielectrics – Sapphire, Rutile, and Strontium Titanate was performed to see which dimensions offered the best sensitivity for the measurements. After deciding the best option, the resonator was constructed and the measurements were done in the laboratory for Rutile and Strontium Titanate.

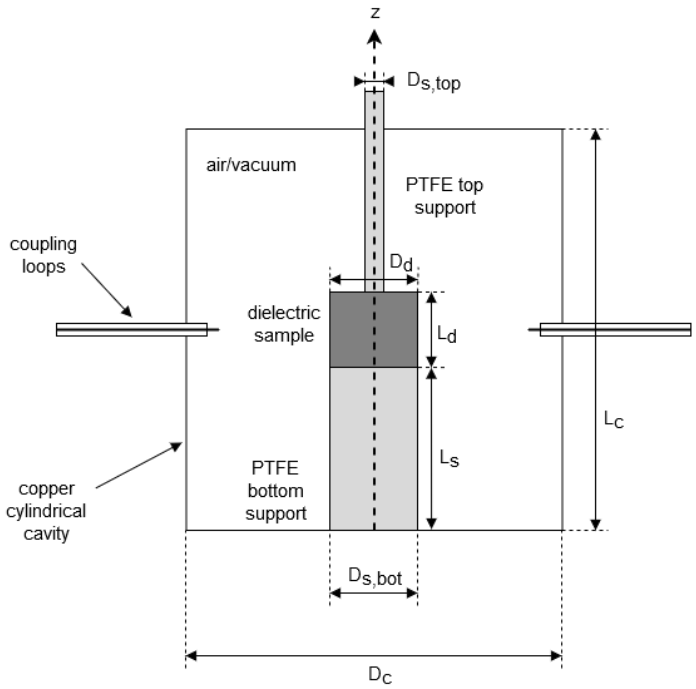

Figure 1.1: Internal diagram of the dielectric resonator. D_d and L_d are the diameter and height of the dielectric sample, respectively. D_c and L_c are the diameter and height of the cavity. $D_{s,bot}$ and L_s are the diameter and height of the bottom PTFE support, and $D_{s,top}$ is the diameter of the top PTFE rod. The height of the top PTFE rod was designed to slightly protrude from the cavity.

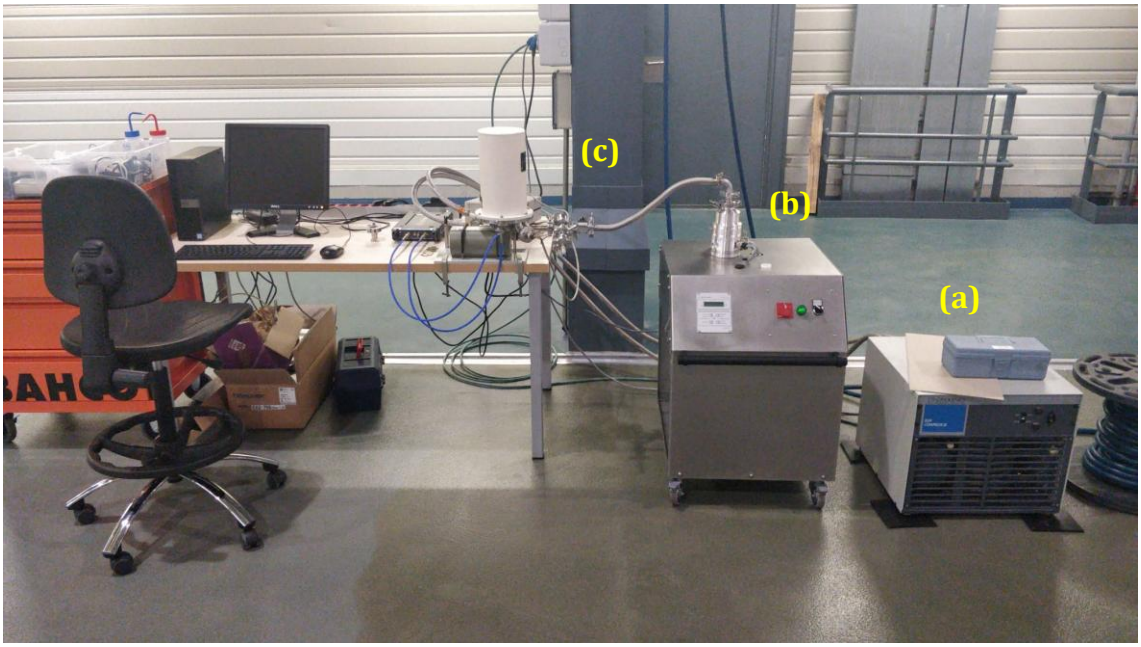

Figure 1.2: Measurement setup. It consists of a cryogenic refrigerator (a), a compact vacuum system (b), a cryostat (c), and a VNA connected to a computer.

1.3. Work plan

This project started with a literature review [6],[8] to get a brief introduction on dielectrics and resonators behavior at cryogenic temperatures and to understand the objectives we wanted to accomplish. After this, knowledge on how to simulate in CST and build a model of the resonator was obtained. Then, a series of simulations was done to obtain the desired design for the resonator. Next, the construction of the resonator was made and the necessary tests performed to obtain the required material properties of the dielectrics under investigation. Finally, about two months were spent on writing the TFG. The milestones of this project are presented in Table 1.1, and its Gantt chart is shown in Fig. 1.3.

Table 1.1: Project milestones

Short title	Milestone / deliverable	Date (week)
Thesis reading Theoretical research		13/3/2020 20/3/2020
Learning CST Cavity dimensions and materials	Cavity design	4/4/2020 15/6/2020
Cavity fabrication Resonator tests	Tests results	14/7/2020 28/7/2020
Report writing TFG report writing	Work Plan and Critical Review TFG report	1/7/2020 11/8/2020

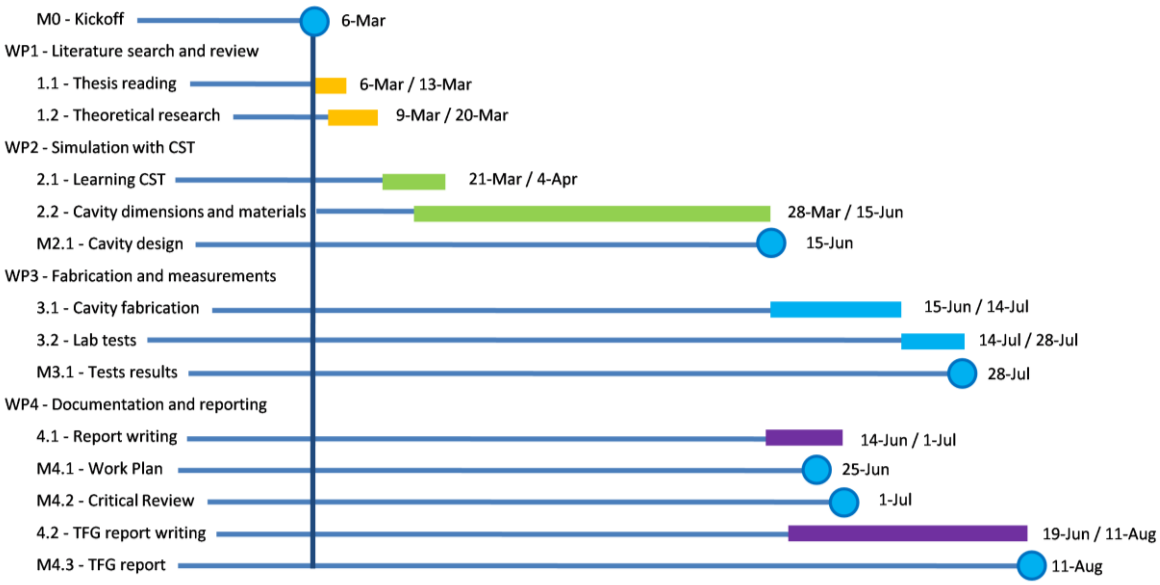

Figure 1.3: Project Gantt chart.

1.4. Incidences

Due to COVID-19, the measurements in the laboratory had to be temporarily suspended (4 months) until the situation came to an acceptable end. The TFG development was adapted to focus on performing simulations through CST, as initially intended but with a wider scope of three different dielectrics.

Also, in July the system and all the equipment dedicated to this project was transferred from UPC to ALBA. During this moving, we had to adapt the water supply needed for refrigerating the compressor. This took one week longer than expected.

2. Resonator basics

2.1. Fundamentals

A **resonator** is a structure that naturally oscillates electromagnetic fields with greater amplitude at certain frequencies (the resonant frequencies) than other frequencies. At resonance, the electromagnetic waves reinforce to form a standing wave.

A **microwave cavity** is a special type of resonator consisting of a closed structure, therefore able to confine electromagnetic fields in the frequency spectrum of 300 MHz – 300 GHz. The cavity can be either hollow or filled with a dielectric to reduce the resonant frequency. In this case it is called a **dielectric resonator**. Due to the higher permittivity of the dielectric compared to its surrounding, it confines most of the electromagnetic fields within it [8].

2.2. Quality factor (Q)

The **quality factor**, or **Q-factor**, is a dimensionless parameter that indicates the energy loss relative to the amount of energy stored within the system. Thus, the higher the Q, the lower the rate of energy loss, and hence, oscillations will be damped less. It is defined by [8]:

$$Q = \omega \frac{average\ energy\ stored}{energy\ loss/second} \quad , \tag{2.1}$$

where $\omega = 2\pi f$ is the angular frequency and f the frequency at which the system operates.

The reciprocal of the quality factor can be thought of as the total loss in the resonating system. The resonator losses can be decomposed into three parts: conductor losses (Q_c) resulting from the losses in the cavity walls which have finite

conductivity; dielectric losses (Q_d) from the losses that the dielectric material introduces; and radiation losses (Q_r) from the losses due to the radiation in case the resonator is not closed. Therefore, the unloaded quality factor (Q_0) can be computed as:

$$\frac{1}{Q_0} = \frac{1}{Q_c} + \frac{1}{Q_d} + \frac{1}{Q_r} \quad . \tag{2.2}$$

For most shielded cavities, the radiation loss is negligible, so the Q_r term can be ignored. If the cavity has no dielectric inside, the Q_d term can also be omitted.

When the resonator is connected to an external circuit, e.g. a VNA, the load introduces additional loss and hence, the term used to describe the total system is the loaded quality factor (Q_L), which is computed as:

$$\frac{1}{Q_L} = \frac{1}{Q_0} + \frac{1}{Q_{ext}} = \frac{1}{Q_c} + \frac{1}{Q_d} + \frac{1}{Q_r} + \frac{1}{Q_{ext}} \quad , \tag{2.3}$$

where Q_{ext} is the external quality factor.

The loaded quality factor is the only parameter in Eq. (2.3) that can be directly measured using a VNA. It is defined as the ratio of the resonant frequency f_0 and the bandwidth Δf at half of the peak power (3 dB bandwidth):

$$Q_L = \frac{f_0}{\Delta f} \quad . \tag{2.4}$$

2.3. Calculating resonator losses

The following section is based on [8].

The losses in the resonator can be calculated by volume integration of the electric and magnetic field energy densities for all regions, and by surface integration of the tangential magnetic field on conducting surfaces. Figure 2.1 shows a representation of the different regions in a multi-dielectric waveguide. Each layer represents a region i, used in Eq. (2.6) to Eq. (2.9).

The resonator losses in the dielectric resonator are the sum of the dielectric and conductor losses, as the radiation losses can be ignored. This separation of individual losses from either dielectric or conductive sources allows these parts to be calculated separately:

$$\frac{1}{Q_0} = \frac{1}{Q_d} + \frac{1}{Q_c} = \frac{W_d}{\omega U} + \frac{W_c}{\omega U} \quad , \tag{2.5}$$

where U is the total stored energy in the resonator, W_d and W_c are the dielectric and conductor losses.

2.3.1. Dielectric losses

The total electric energy (U_{el}) in a dielectric can be found by integrating the modulus of the electric energy density over the volume of the resonator:

$$U_{el} = \sum_i U_{el,i} = \frac{1}{2} \sum_i \int_{V_i} \varepsilon_i' \boldsymbol{E} \cdot \boldsymbol{E}^* dV_i \quad , \tag{2.6}$$

where i is each partial region of the resonator. The complex electric permittivity for region i is $\varepsilon_i = \varepsilon_i' + i\varepsilon_i''$.

Similarly, the dielectric dissipation for each region can be found as:

$$W_{d,i} = \frac{\omega}{2} \int_{V_i} \varepsilon_i'' \boldsymbol{E} \cdot \boldsymbol{E}^* dV_i \quad . \tag{2.7}$$

Then, the dielectric loss for a region i can be written:

$$\frac{1}{Q_{d,i}} = \frac{W_{d,i}}{\omega U_{el}} = \frac{tan\,\delta_i U_{el,i}}{U_{el}} = P_{d,i}\, tan\,\delta_i \quad , \tag{2.8}$$

where the loss tangent, $\tan\delta = \frac{\varepsilon''}{\varepsilon'}$, is the ratio of imaginary and real part of the complex permittivity.

The **electric filling factor** ($P_{d,i}$) for a region i is then introduced, defined as:

$$P_{d,i} = \frac{U_{el,i}}{U_{el}} \quad . \tag{2.9}$$

It indicates the fraction of electric field energy stored in the dielectric in relation to the total energy stored in the cavity resonator.

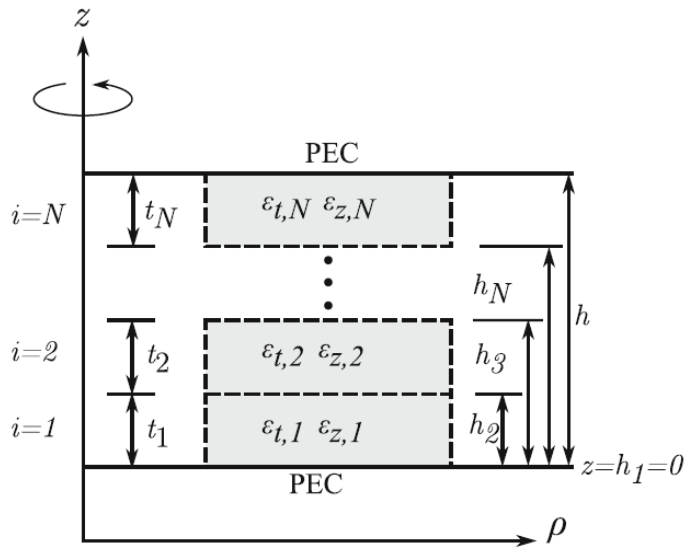

Figure 2.1: The anisotropic dielectric-loaded parallel plate waveguide. There are N layers of dielectric each with thickness t_i, where $i = 1, 2, \dots, N$. The multilayer is between perfect electric conductors (PEC). Figure taken from [8].

2.3.2. Conductor losses

In resonator structures, conductor losses occur on metallic surfaces that have finite electrical conductivity. The losses for a particular metallic surface l within a resonator can be calculated as:

$$\frac{1}{Q_{c,l}} = \frac{W_{c,l}}{\omega U} \quad , \tag{2.10}$$

where $W_{c,l}$ is the conductive dissipation for a surface l.

The dissipation $W_{c,l}$ is found by integrating the tangential magnetic field over the conductive surface l:

$$W_{c,l} = \frac{1}{2} R_{S_l} \int_{S_l} |\boldsymbol{H}_t|^2 dS \quad , \tag{2.11}$$

with the surface resistance R_{S_l} given by:

$$R_{S_l} = (f \mu_0 \pi \rho_l)^{\frac{1}{2}} \quad , \tag{2.12}$$

where μ_0 is the vacuum magnetic permeability and ρ_l the resistivity of the metal.

The total stored energy can be expressed similarly to the previously calculated electric energy in Eq. (2.6) over the magnetic energy (U_{mag}):

$$U_{mag} = \frac{1}{2}\mu_0 \int_V \boldsymbol{H} \cdot \boldsymbol{H}^* dV \quad . \tag{2.13}$$

The total conductor loss is then computed as:

$$\frac{1}{Q_{c,l}} = \frac{W_{c,l}}{\omega U_{mag}} = \frac{R_{S_l} \int_{S_l} |\boldsymbol{H}_t|^2 dS}{\omega\mu_0 \int_V \boldsymbol{H} \cdot \boldsymbol{H}^* dV} = \frac{R_{S_l}}{G} \quad , \tag{2.14}$$

which introduces the **geometric factor** (G), for a surface l.

$$G_l = \omega\mu_0 \frac{\int_V \boldsymbol{H} \cdot \boldsymbol{H}^* dV}{\int_{S_l} |\boldsymbol{H}_t|^2 dS} \quad . \tag{2.15}$$

It represents the ratio of cavity volume to surface area which increases with increasing cavity size for a fixed frequency, and is given in units of "ohms".

2.4. Coupling factors for two-ports resonators

2.4.1. S-Parameters

Scattering parameters or S-Parameters can be described as the parameters that relate the incoming and outgoing waves to the device under test (DUT) which characterizes it from the exterior. They are complex, frequency-dependent and can be stored as reflection or transmission coefficients.

S-Parameters are usually displayed in a matrix format, with the number of rows and columns equal to the number of ports. For the S-Parameter S_{ij} the subscript "*j*" stands for the port that is excited (the input port), and the subscript "*i*" is for the output port. Here are the S-matrices for one, two, and three-port networks:

$$(S_{11})(one-port) \quad \begin{pmatrix} S_{11} & S_{12} \\ S_{21} & S_{22} \end{pmatrix}(two-port) \quad \begin{pmatrix} S_{11} & S_{12} & S_{13} \\ S_{21} & S_{22} & S_{23} \\ S_{31} & S_{32} & S_{33} \end{pmatrix}(three-port) \quad . \tag{2.16}$$

In this work, we are focused on the use of a dielectric resonator with two ports coupling. Naturally, we will focus in the following only on the two-port matrix. The relationship between the reflected, transmitted and incident power waves, shown in Fig. 2.2, and the S-Parameter matrix for a two-port network (Eq. (2.16)) is the following [8]:

$$\begin{pmatrix} b_1 \\ b_2 \end{pmatrix} = \begin{pmatrix} S_{11} & S_{12} \\ S_{21} & S_{22} \end{pmatrix} \begin{pmatrix} a_1 \\ a_2 \end{pmatrix} \quad , \tag{2.17}$$

where a_1 and a_2 are the incident power waves of ports 1 and 2 and b_1 and b_2 the reflected waves. The S-Parameters have the following descriptions:

- S_{11} is the forward reflection coefficient
- S_{12} is the forward transmission coefficient
- S_{21} is the reverse transmission coefficient
- S_{22} is the reverse reflection coefficient

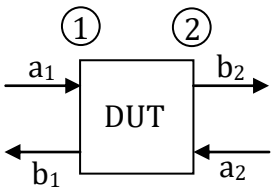

Figure 2.2: Incident, transmitted and reflected power waves upon and from a two-port device under test.

S-Parameters are usually measured with the help of a VNA and stored in the Touchstone format text file (.snp), where n indicates the number of ports of the system. Figure 2.3 shows an example of how the S-Parameters of a .s2p file are distributed for a two-port device. The resonant frequency is obtained from the maximum of the S_{21} parameter. It can be seen that S_{21} equals S_{12} in this example. The loaded quality factor can be extracted by using Eq. (2.4).

2.4.2. Coupling coefficients

The following subsection, and its equations, is based on [6].

The coupling coefficients β_1 and β_2 of a two-port resonating system relate the unloaded quality factor with the external quality factor from each port. The coupling coefficients can be calculated from the four S-Parameters measured using a VNA at the resonant frequency:

$$\beta_1 = \frac{1 - S_{11}}{S_{11} + S_{22}} \quad , \tag{2.18}$$

$$\beta_2 = \frac{1 - S_{22}}{S_{11} + S_{22}} \quad , \tag{2.19}$$

$$S_{21} = S_{12} = \frac{2\sqrt{\beta_1 \beta_2}}{1 + \beta_1 + \beta_2} \quad . \tag{2.20}$$

Here, S_{11} and S_{22} are the magnitude values of the minimum of the resonance curve, as can be seen in Fig. 2.3, respectively.

Q_0 can be calculated from the measured coupling coefficients and Q_L as:

$$Q_0 = (1 + \beta_1 + \beta_2) Q_L \quad . \tag{2.21}$$

If the input and output couplings β_1 and β_2 are both equal and weak, then the transmission response should be symmetric, the resonant frequency occurs at the peak maximum and the coupling coefficient can be evaluated as:

$$\beta = \beta_1 = \beta_2 = \frac{1}{2} \cdot \frac{S_{21}}{1 - S_{21}} \quad . \tag{2.22}$$

From Eqs. (2.21) and (2.22), the unloaded quality factor can then be calculated from the measured Q-factor and the transmission coefficient S_{21}:

$$Q_0 = \frac{Q_L}{1 - |S_{21}|} \quad . \tag{2.23}$$

If S_{21} is small, meaning below -30 dB, then according to Eq. (2.23) we can assume that Q_0 is approximately equal to Q_L. Naturally, the best for the measurements is to stay with a low coupling signal below this boarder, as it allows you to take directly the loaded Q-factor as the unloaded Q-factor.

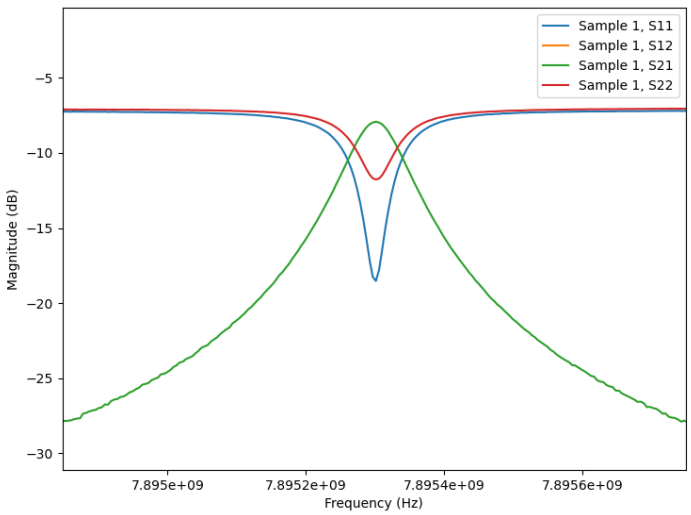

Figure 2.3: Example of the measured S-Parameters of a two-port device under test, having an asymmetric strong coupling.

3. Simulations

3.1. CST Studio Suite software

CST Studio Suite [7] was used in this project in order to perform several electromagnetic simulations of the dielectric resonator. CST offers multiple electromagnetic simulation solvers for high frequency tasks. The solvers used for this work were the "Frequency Domain Solver" and the "Eigenmode Solver", which allowed us to obtain the S-Parameters (coupling strength) of the cavity and the quality factor and resonant frequency for different modes, respectively. With this, we were able to see how changing certain parameters, like the diameter or the height of the cavity, affected the resonator performance.

3.1.1. Eigenmode Solver

The Eigenmode Solver is a simulation tool suited best for closed resonant structures. It is able to calculate modal field distributions in loss free or lossy structures. This solver has been used to calculate all the resonant modes of the cavity and the corresponding unloaded Q-factors, as well as the geometric factors Eq. (2.15) and filling factors Eq. (2.9) of the resonator. A sweep can be made to see how these parameters change for different resonator sizes. It was also used to check that the modes are well separated, so no other modes interfere with the modes of interest.

For this solver, the modelling of the coupling loops is not necessary, as it solves Maxwell equations numerically in each mesh cell, see Fig. 3.1. Therefore, a simple model of a closed cylindrical resonator without any walls and with the background set as copper, as shown in Fig. 3.2 and Fig. 3.3, is sufficient. The cavity is modelled by defining the empty space of the resonance region (indicated in blue in Fig. 3.1). The dielectrics are inserted within that region, support seen in gray in Fig. 3.3 and dielectric under investigation in dark blue.

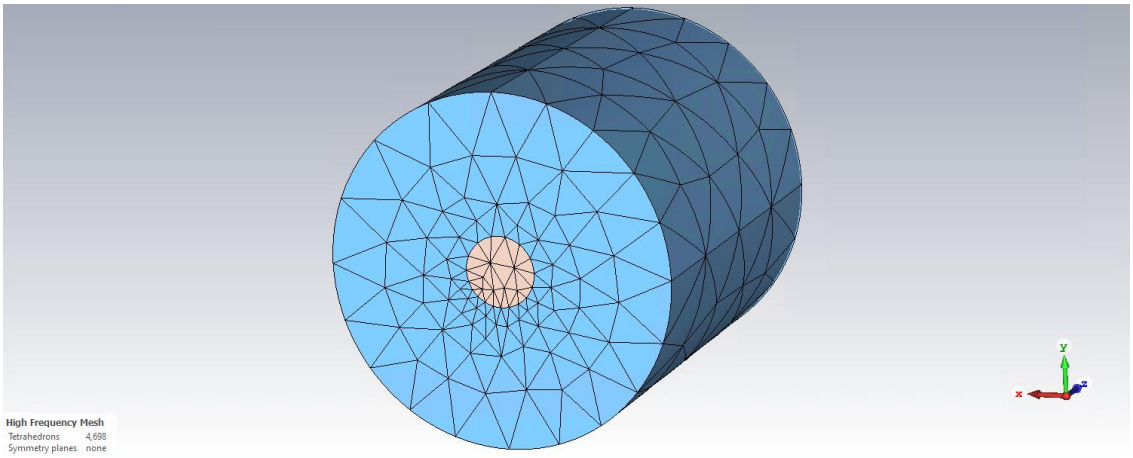

Figure 3.1: Mesh view of the dielectric resonator using tetrahedrons for the numerical calculation. The mesh gets denser the higher the permittivity of the region.

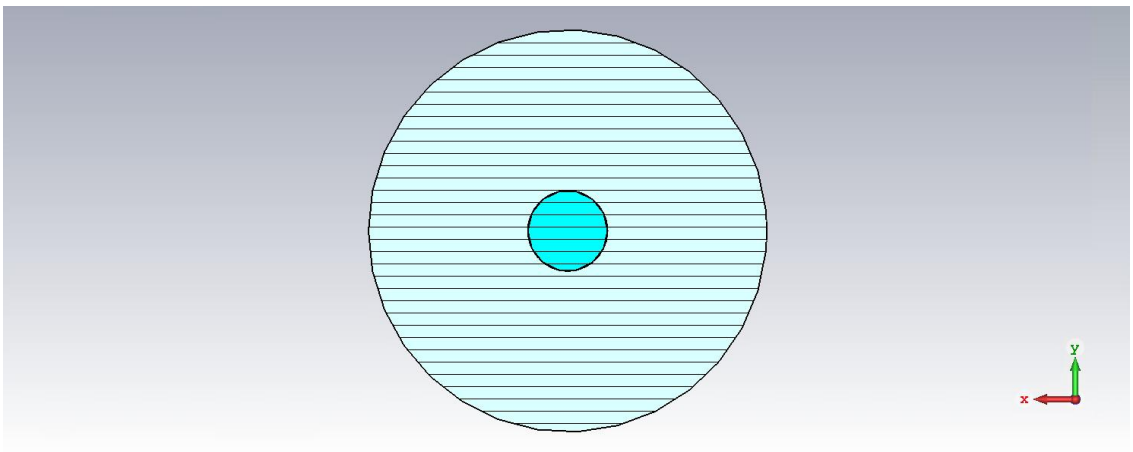

Figure 3.2: Cross section of the transversal plane of dielectric resonator without ports.

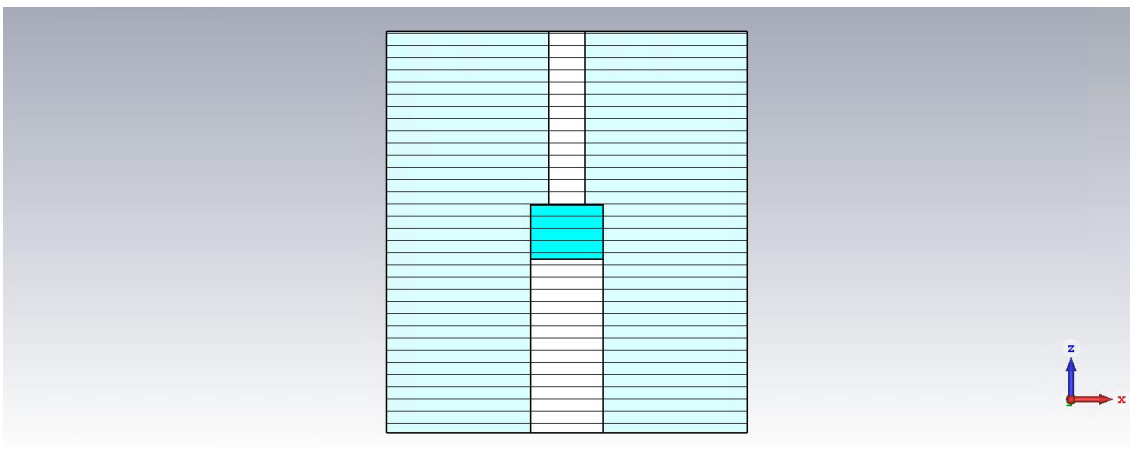

Figure 3.3: Cross section of the frontal plane of dielectric resonator without ports.

3.1.2. Frequency Domain Solver

The Frequency Domain Solver is a tool for more general purposes, used to simulate multi-port systems in the frequency domain. It is necessary to define two ports, see Fig. 3.4 indicated as red squares at the coaxial ending, through which the electromagnetic fields are introduced into the simulations. Hence, a full modelling is required. This includes the cavity walls, the coaxial cables, and the coupling loops, see Fig. 3.5 and Fig. 3.6. This solver has been used to calculate the S-Parameters of the device and to define the right coupling position to the modes of interest being below -30 dB.

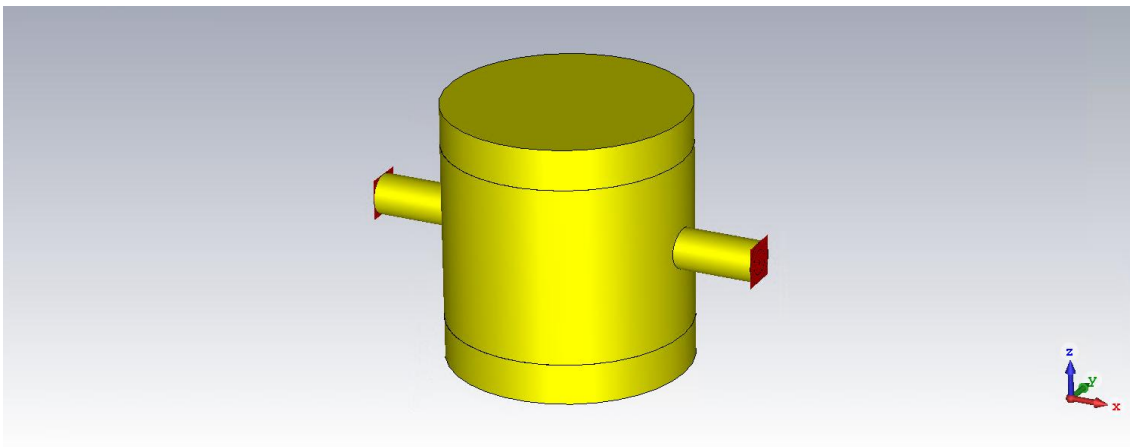

Figure 3.4: External view of the dielectric resonator. The two ports can be seen at the ends of the coaxial cable.

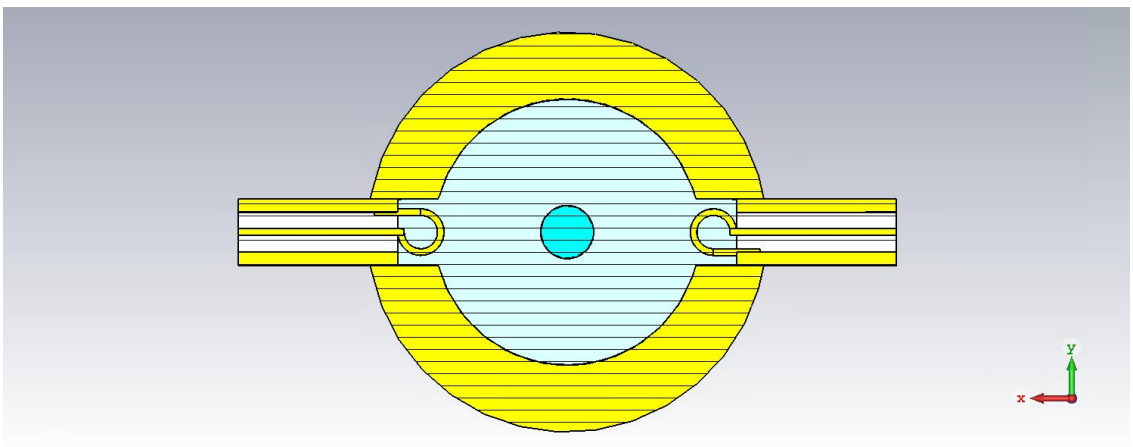

Figure 3.5: Cross section of transversal plane of the dielectric resonator with the two ports and coupling loops.

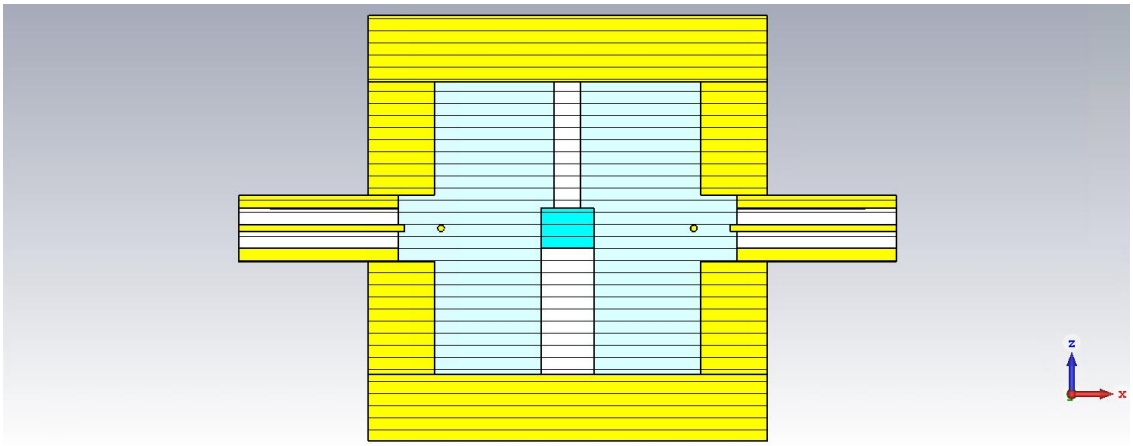

Figure 3.6: Cross section of frontal plane of the dielectric resonator with the two ports and coupling loops.

3.2. Definitions of $TE_{01\delta}$ and $TM_{01\delta}$ modes

Even though CST computes and represents all modes present within a certain frequency range, it does not define which they are, and they must be visually interpreted. For this reason, a good understanding of the desired transverse modes is required.

A **transverse mode** is a resonant mode whose electric and/or magnetic field is completely transversal to the direction of propagation. Depending on the presence of electric or magnetic fields in the axis direction, the modes in waveguides can be further classified as:

- Transverse electromagnetic (TEM) modes: Neither electric nor magnetic field in the direction of propagation.
- Transverse electric (TE) modes: No electric field in the direction of propagation. These are sometimes called *H modes* because there is only a magnetic field along the direction of propagation.
- Transverse magnetic (TM) modes: No magnetic field in the direction of propagation. These are sometimes called *E modes* because there is only an electric field along the direction of propagation.
- Hybrid modes: Non-zero electric and magnetic fields in the direction of propagation.

In the cylindrical coordinate system, the mode numbers are designated by three suffix numbers attached to the mode type, such as TE_{mnl} and TM_{mnl}. The indexes *m*, *n*, and *l* stand for the number of wave patterns in the azimuth, radial, and axial components, respectively.

The dielectric resonator to study in Fig. 3.6 is a cylindrical cavity constructed from a section of circular waveguide shorted at both ends. The dominant mode, which means the mode with the lowest cutoff frequency (the lowest frequency for which a mode will propagate in it) for the TE-mode is the TE_{111} mode, while the dominant TM-mode is the TM_{010} mode [8]. The modes of the circular metallic cavity of interest nevertheless are the TE_{011} and TM_{010} modes. These modes will be excited depending on the orientation of the coupling loops; when the loops are placed horizontally oriented, they will excite the magnetic field z-component (H_z) and the TE_{011} mode will be present. On the other hand, when the loops are placed vertically oriented, the azimuth component of the magnetic field (H_ϕ) will be the one exited, and the TM_{010} mode will be present.

The indices in the TE_{011} mode for the circular cavity resonator mean it has 0 maximums in the azimuth electric field component, 1 maximum in the radial component and 1 maximum in the axial component in the electric field, as can be seen in Fig. 3.7 (a) and (b). The TE-mode has the advantage of having only an azimuth component for the e-field, so the perpendicular component of the permittivity and loss tangent can be extracted directly.

To obtain the parallel component, the TM-mode is used, which has a radial and axial component of the e-field when placed the dielectric sample and, therefore, the perpendicular and parallel components of the parameters affect the results. The TM_{010} mode has 0 maximums in the azimuth electric field component, 1 maximum in the radial component and 0 maximums in the axial component in the magnetic field, as can be seen in Fig. 3.8 (a) and (b).

In the case of including several dielectrics, the field distribution changes and the modes are actually $TE_{01\delta}$ and $TM_{01\delta}$ modes, which are analogous to the TE_{011} and TM_{010} modes of a circular empty metallic cavity, respectively. The difference resides in a denser field near the centered dielectric, which can be seen in Fig. 3.7 (c) and (d) and Fig. 3.8 (c) and (d). Due to the abrupt change of permittivity between the dielectric and the air/vacuum or PTFE, the fields that propagate through the

dielectric will be cut off around it, producing a variation in the z-component of the magnetic field (H_z). This variation is denoted in the symbol $\delta = \frac{2L}{\lambda_g} < 1$, where L is the height of the dielectric cylinder and λ_g is the guide wavelength of the TE_{01} dielectric waveguide mode [8]. Because of this field variation, the geometric and filling factors must be simulated in CST, as they cannot be solved analytically.

3.3. Computation of relative loss distribution for cavity design

In order to properly measure the dielectric loss tangent with the least possible error, we need to ensure that the dielectric under investigation is the main contributor to the losses created within the resonator.

First, the expected values of the loss tangent and relative permittivity of the dielectric under investigation and the support material and the resistivity of the copper are obtained through literature research, see Tab 3.1. From these values, a survey for different cavity sizes is performed to see the distribution of losses in each case. Finally, the optimal size for the cavity is decided depending on the contribution of the dielectric to the losses in both modes; at room and cryogenic temperature.

The initial aim was to obtain a loss for the dielectric under test with a minimum percentage of approximately 90% of the total loss, at room and cryogenic temperatures. This ensures a better sensitivity on the measurements, since it reduces the error that the estimation of the geometric and filling factors, loss tangent of the support material, and surface resistance of the cavity material can cause. The cavity material used is copper, with a conductivity of $\sigma = 5.95 \cdot 10^7\ S/m$ [9] at room temperature (300K) and $\sigma = 5.95 \cdot 10^8\ S/m$ at cryogenic temperature (50K), obtained from the residual-resistance ratio $RRR = \frac{\rho|_{300K}}{\rho|_{50K}} = 10$ [10]. For the material support, PTFE was chosen, and the dielectrics simulated were Titanium Dioxide (Rutile), Aluminium Oxide (Sapphire), and Strontium Titanate. Some of the dielectrics are anisotropic, which means, their material properties vary depending on whether they are observed perpendicular or parallel to the z-axis of the cavity.

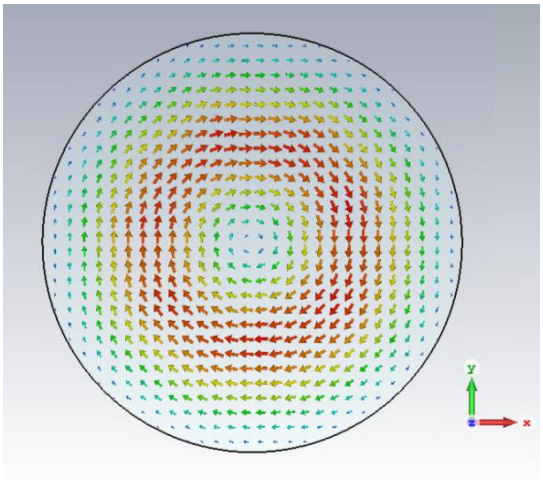

(a) e-field

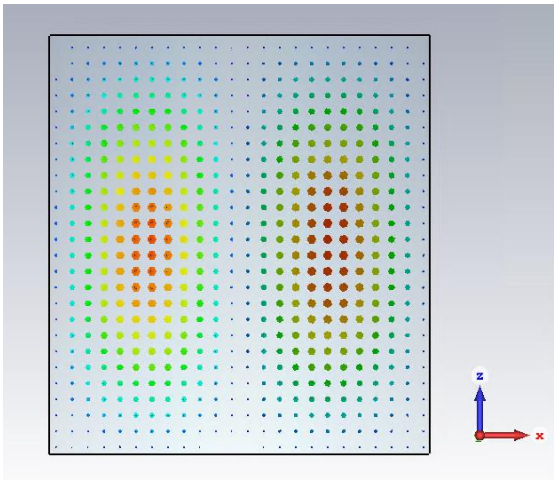

(b) e-field

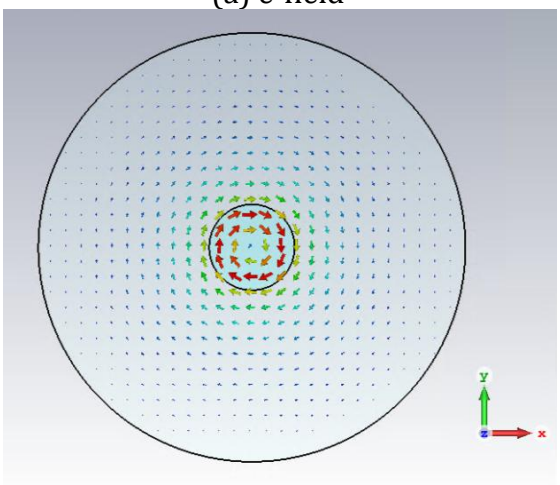

(c) e-field

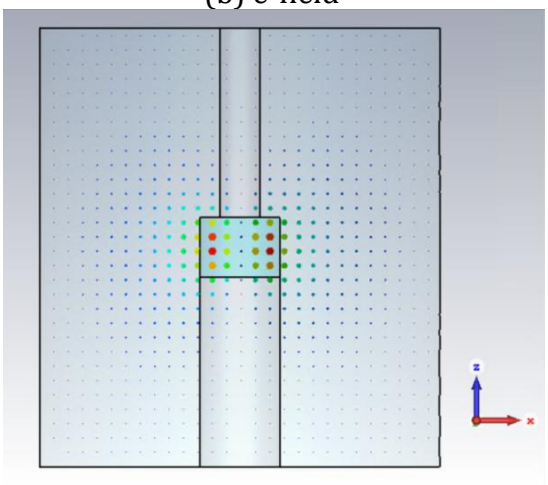

(d) e-field

Figure 3.7: CST simulations of the resonator. (a) XY plane of electric field for the TE_{011} mode in an empty cavity. (b) XZ plane of electric field for the TE_{011} mode in an empty cavity. (c) XY plane of electric field for the $TE_{01\delta}$ mode in a dielectric filled cavity. (d) XZ plane of electric field for the $TE_{01\delta}$ mode in a dielectric filled cavity.

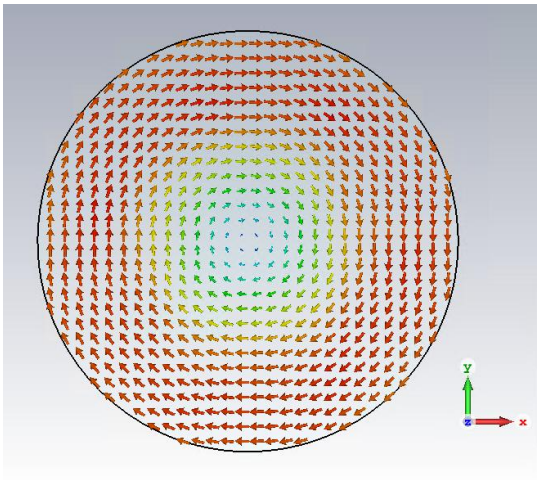

(a) h-field

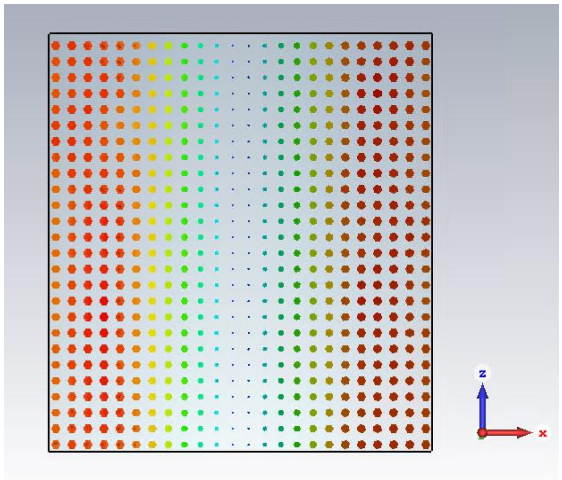

(b) h-field

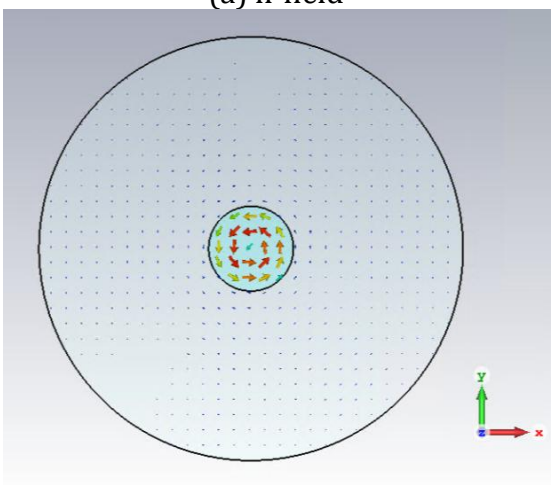

(c) h-field

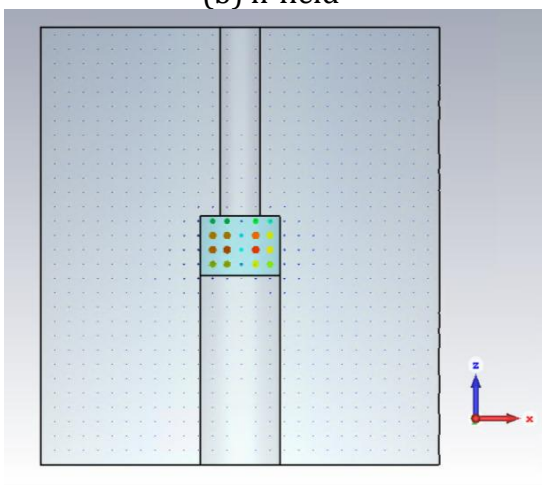

(d) h-field

Figure 3.8: CST simulations of the resonator. (a) XY plane of magnetic field for the TM_{010} mode in an empty cavity. (b) XZ plane of magnetic field for the TM_{010} mode in an empty cavity. (c) XY plane of magnetic field for the $TM_{01\delta}$ mode in a dielectric filled cavity. (d) XZ plane of magnetic field for the $TM_{01\delta}$ mode in a dielectric filled cavity.

Table 3.1: Parameters of the dielectrics of interest. Values taken from [6],[11]-[14].

		Room temperature	**50 K**
Titanium Dioxide (Rutile) - $Ti0_2$	$\tan\delta_\perp$	$5.55 \cdot 10^{-5}$	$2 \cdot 10^{-6}$
	$\tan\delta_\parallel$	$6.82 \cdot 10^{-5}$	$2 \cdot 10^{-6}$
	$\varepsilon_\perp$	86	112
	$\varepsilon_\parallel$	163	245
Aluminium Oxide (Sapphire) - Al_2O_3	$\tan\delta_\perp$	$5.35 \cdot 10^{-6}$	$2.2 \cdot 10^{-8}$
	$\tan\delta_\parallel$	$3.91 \cdot 10^{-6}$	$1.3 \cdot 10^{-8}$
	$\varepsilon_\perp$	9.395	9.25
	$\varepsilon_\parallel$	11.592	11.35
Strontium Titanate - $SrTiO_3$	$\tan\delta_\perp$	$4.21 \cdot 10^{-4}$	$4.521 \cdot 10^{-4}$
	$\tan\delta_\parallel$	$4.21 \cdot 10^{-4}$	$4.521 \cdot 10^{-4}$
	$\varepsilon_\perp$	398.86	3179
	$\varepsilon_\parallel$	398.86	3179
Polytetrafluoroethylene (PTFE)	$\tan\delta_\perp$	$2 \cdot 10^{-4}$	$3 \cdot 10^{-6}$
	$\tan\delta_\parallel$	$2 \cdot 10^{-4}$	$3 \cdot 10^{-6}$
	$\varepsilon_\perp$	2.1	2.1
	$\varepsilon_\parallel$	2.1	2.1

From these parameters, the resonator size has been determined to be $D_C = 20$ mm and a height of $L_C = 22$ mm. Figure 3.9 shows the internal configuration of the dielectric resonator with the final dimensions. These values resulted as a balance between having the total losses predominantly in the dielectric under study versus the mechanical limits of supporting correctly the dielectric sample in the center. Clearly, one could think, the larger the distance between dielectric under study and metallic housing, the lower is the conductive loss contribution. Therefore, the higher the sensitivity. Nevertheless, it was observed that increasing the height of the cavity increased the contribution of the dielectric under investigation, but increasing the diameter, on the one hand, improved the performance of the resonator for the TE-mode, while it made it worse for the TM-mode. For the case study of the dimensions Rutile was used as the medium dielectric between Sapphire (low losses and low permittivity) and Strontium Titanate (high losses and high permittivity). From the dielectrics simulated, Rutile gave acceptable results in the sensibility, having around 90% of dielectric losses in the TE-mode. The Strontium Titanate also gave very good sensibility, as the dielectric losses were around 99%. Finally, it was seen that for Sapphire the dielectric properties could not be properly measured, since it had very few losses that represented around 3%.

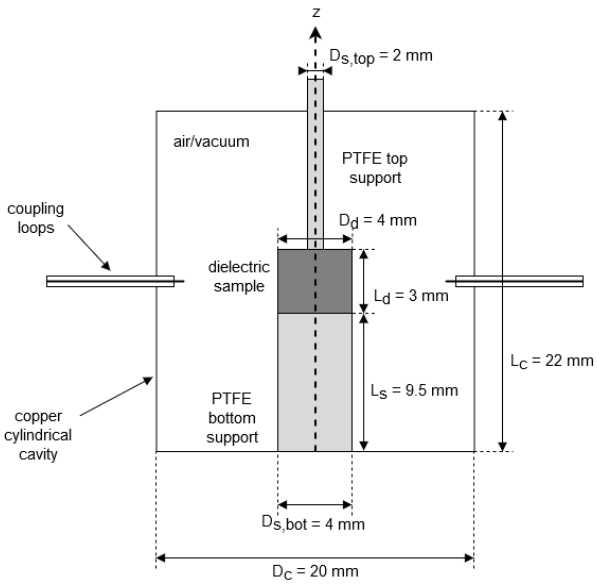

Figure 3.9: Dielectric resonator dimensions.

3.4. Computation of geometric and filling factors with CST simulations

In order to experimentally measure the loss tangent of the dielectric of interest, it is necessary to obtain the filling factor from Eq. (2.9) of the dielectric under investigation and PTFE supports. The geometric factor of the cavity, from Eq. (2.15), also needs to be obtained to define the conductor losses. They can be simulated and are independent of the loss tangent values of the dielectrics and surface resistance of the cavity material, but depends on the permittivity of the dielectrics. The procedure to obtain their values consists of using CST in combination with Eqs. (3.1) and (3.2).

Depending on which mode we are looking at, the components of the electric field vary. Hence, the formulas for the $TE_{01\delta}$ and $TM_{01\delta}$ modes will differ, as the TE-mode only has an azimuth component of the electric field while in the TM-mode has radial and axial components. The formulas are the following [6]:

For the $TE_{01\delta}$ mode:

$$\frac{1}{Q_0} = P_{d,\phi} \tan\delta_{\perp} + P_{s,\phi} \tan\delta_{s,\perp} + \frac{R_s}{G} \quad , \tag{3.1}$$

and for the $TM_{01\delta}$ mode:

$$\frac{1}{Q_0} = P_{d,\rho} \tan\delta_{\perp} + P_{d,z} \tan\delta_{\parallel} + P_{s,\rho} \tan\delta_{s,\perp} + P_{s,z} \tan\delta_{s,\parallel} + \frac{R_s}{G} \quad , \tag{3.2}$$

where $P_{d,\phi}$,$P_{d,\rho}$, and $P_{d,z}$ are the azimuth, radial, and axial components of the filling factor of the dielectric under test. $P_{s,\phi}$, $P_{s,\rho}$, and $P_{s,z}$ are the azimuth, radial, and axial components of the filling factor of the support material. The perpendicular and parallel components of the loss tangent of the dielectric under test are $\tan\delta_{\perp}$ and $\tan\delta_{\parallel}$. The perpendicular and parallel components of loss tangent of the support material are $\tan\delta_{s,\perp}$ and $\tan\delta_{s,\parallel}$. These formulas assume an anisotropic dielectric and support material. If the support material is isotropic, Eq. (3.2) results in:

$$\frac{1}{Q_0} = P_{d,\rho}\tan\delta_{\perp} + P_{d,z}\tan\delta_{\parallel} + P_s\tan\delta_s + \frac{R_s}{G} \quad , \tag{3.3}$$

where P_s is the filling factor of the support material and $\tan\delta_s$ is the isotropic loss tangent of the support material.

If the dielectric under investigation is also isotropic, Eq. (3.2) would be:

$$\frac{1}{Q_0} = P_d\tan\delta + P_s\tan\delta_s + \frac{R_s}{G} \quad , \tag{3.4}$$

where P_d is the filling factor if the dielectric and $\tan\delta$ is the isotropic loss tangent of the dielectric under investigation.

The method to simulate the geometric and filling factors is to put the loss tangent of the materials and the resistivity of the cavity walls to zero, except for the element to be determined, and from there, extract the unknown parameter. For example, in order to get the value of the filling factor of the dielectric under study, the loss tangent of the support material and the resistivity of the cavity walls are set zero. After doing this, and obtaining the resulting Q_0, we use Eq. (3.5) to get the unknown parameter $P_{d,\phi}$. This will be repeated for all geometric and filling factors.

The combinations needed in order to measure all the required filling factors and geometric factor are the following:

For the $TE_{01\delta}$ mode:

- from Eq. (3.1), if $\tan\delta_{s,\perp} = R_S = 0$:

$$\frac{1}{Q_0} = P_{d,\phi}\tan\delta_{\perp} \quad , \tag{3.5}$$

- if $\tan\delta_{\perp} = R_S = 0$:

$$\frac{1}{Q_0} = P_{s,\phi}\tan\delta_{s,\perp} \quad , \tag{3.6}$$

- and if $\tan\delta_{\perp} = \tan\delta_{s,\perp} = 0$:

$$\frac{1}{Q_0} = \frac{R_s}{G} \quad . \tag{3.7}$$

For the $TM_{01\delta}$ mode:

- from Eq. (3.2), if $\tan\delta_{\parallel} = \tan\delta_{s,\perp} = \tan\delta_{s,\parallel} = R_S = 0$:

$$\frac{1}{Q_0} = P_{d,\rho}\tan\delta_{\perp} \quad , \tag{3.8}$$

- if $\tan\delta_{\perp} = \tan\delta_{s,\perp} = \tan\delta_{s,\parallel} = R_S = 0$:

$$\frac{1}{Q_0} = P_{d,z}\tan\delta_{\parallel} \quad , \tag{3.9}$$

- if $\tan\delta_{\perp} = \tan\delta_{\parallel} = \tan\delta_{s,\parallel} = R_S = 0$:

$$\frac{1}{Q_0} = P_{s,\rho}\tan\delta_{s,\perp} \quad , \tag{3.10}$$

- if $\tan\delta_{\perp} = \tan\delta_{\parallel} = \tan\delta_{s,\perp} = R_S = 0$:

$$\frac{1}{Q_0} = P_{s,z}\tan\delta_{s,\parallel} \quad , \tag{3.11}$$

- and if $\tan\delta_{\perp} = \tan\delta_{\parallel} = \tan\delta_{s,\perp} = \tan\delta_{s,\parallel} = 0$:

$$\frac{1}{Q_0} = \frac{R_s}{G} \quad . \tag{3.12}$$

The simulations have been done for two temperatures; room temperature and 50 K; first, for an empty cavity, and second, for a cavity filled with the dielectric sample and supports. In each simulation we will look at both modes.

For the empty cavity at room temperature, the conductivity used for the copper is mentioned in Sec. 3.3. The resonant frequency of the TE_{011} mode was found to be $f_0 = 19.5111\ GHz$, so the surface resistance from Eq. (2.12) is $R_S = 35.97\ m\Omega$. The unloaded Q-factor obtained is $Q_0 = 21237$, and this results from Eq. (3.7) on a geometric factor of $G = 764\ \Omega$. For the TM_{010} mode, the resonant frequency is at $f_0 = 11.4743\ GHz$, giving a surface resistance of $R_S = 27.59\ m\Omega$. The unloaded quality factor is $Q_0 = 11245$, so from Eq. (3.12) the geometric factor is $G = 310\ \Omega$.

For the resonator with the Rutile sample at room temperature, the parameters used are written in Tab. 3.1. The $TE_{01\delta}$ mode was found at a resonant frequency of $f_0 = 7.5966\ GHz$, leaving a surface resistance of $R_S = 22.45\ m\Omega$. The Q-factor has a

value of $Q_0 = 17940$. If all the losses except the conductor losses are put to zero, the Q-factor obtained is $Q_0 = 1055200$, which from Eq. (3.7) gives the geometric factor $G = 23997\ \Omega$. If only the PTFE losses are left, the Q-factor is $Q_0 = 2533800$, and from Eq. (3.6) the filling factor for the PTFE is $P_s = 0.001973$. If only Rutile losses are present, the resulting Q-factor is $Q_0 = 18435$, which from Eq. (3.5) results in a filling factor of the azimuth component of the dielectric $P_{d,\phi} = 0.9774$.

For the $TM_{01\delta}$ mode, we proceed similarly. The resonant frequency is found at $f_0 = 8.8421\ GHz$, and the surface resistance obtained is $R_S = 24.22\ m\Omega$. The Q-factor obtained is $Q_0 = 15268$. If only the conductive losses are present, the Q-factor obtained is $Q_0 = 850580$, and from Eq. (3.12) the geometric factor is $G = 20866\ \Omega$. If the PTFE losses are the only losses, the resulting Q-factor is $Q_0 = 265480$, obtaining a filling factor of the PTFE supports of $P_s = 0.01883$ from Eqs. (3.10) and (3.11). For Rutile losses, if only the perpendicular component of the loss tangent is left, then from Eq. (3.8) we obtain the filling factor with radial component of $P_{d,\rho} = 0.3430$. Instead, with only the parallel component of the loss tangent, from Eq. (3.9) we obtain a z-component of the filling factor of $P_{d,z} = 0.6074$.

In the following tables, the simulated parameters for the different dielectric samples under study are summarized. At room temperature, the simulation results are shown in Tab. 3.2 for the empty cavity and in Tab. 3.3 for the dielectric resonator. At the cryogenic temperature of 50 K, the simulation results for the empty cavity and dielectric resonator are shown in Tab. 3.4 and Tab. 3.5, respectively.

Table 3.2: Parameters simulated in CST for the TE_{011} and TM_{010} mode of the empty cavity at room temperature.

mode	TE_{011}	TM_{010}
f_0 [GHz]	19.5244	11.4753
Q_0	18665	10944
R_S [mΩ]	35.99	27.59
G [Ω]	672	302

Table 3.3: Parameters simulated in CST for the $TE_{01\delta}$ and $TM_{01\delta}$ mode of the resonator filled with the dielectrics under investigation at room temperature.

	Titanium Dioxide (Rutile)		Aluminium Oxide (Sapphire)		Strontium Titanate	
mode	$TE_{01\delta}$	$TM_{01\delta}$	$TE_{01\delta}$	$TM_{01\delta}$	$TE_{01\delta}$	$TM_{01\delta}$
f_0 [GHz]	7.5987	8.8422	18.5567	10.5829	3.5533	5.1991
Q_0	17990	15289	25159	8171.9	2391.1	2399.8
R_S [mΩ]	22.74	24.53	35.08	26.49	15.35	18.57
G [Ω]	23997	20866	1011	328	17356	1079068
P_s	0.001973	0.01883	0.01941	0.2083	$4.027 \cdot 10^{-4}$	0.002305
$P_{d,\phi}$	0.9774	–	0.2185	–	0.9911	–
$P_{d,\rho}$	–	0.3430	–	0.001213	–	0.2297
$P_{d,z}$	–	0.6074	–	0.02181	–	0.7590

Table 3.4: Parameters simulated in CST for the TE_{011} and TM_{010} mode of the empty cavity at 50 K.

mode	TE_{011}	TM_{010}
f_0 [GHz]	19.5244	11.4753
Q_0	59025	34608
R_S [mΩ]	11.38	8.72
G [Ω]	672	302

Table 3.5: Parameters simulated in CST for the $TE_{01\delta}$ and $TM_{01\delta}$ mode of the resonator filled with the dielectrics under investigation at 50 K.

	Titanium Dioxide (Rutile)		Aluminium Oxide (Sapphire)		Strontium Titanate	
mode	$TE_{01\delta}$	$TM_{01\delta}$	$TE_{01\delta}$	$TM_{01\delta}$	$TE_{01\delta}$	$TM_{01\delta}$
f_0 [GHz]	6.6734	7.4494	18.5892	10.5846	1.26115	1.84701
Q_0	444670	490730	88046	38198	2216.2	2218.4
R_S [mΩ]	6.74	7.12	11.10	8.38	2.89	3.50
G [Ω]	24120	132605	983	328	6739	$4.934 \cdot 10^{7}$
P_s	0.001492	0.009465	0.01949	0.2088	$5.012 \cdot 10^{-5}$	$2.446 \cdot 10^{-4}$
$P_{d,\phi}$	0.9825	–	0.2088	–	0.9963	–
$P_{d,\rho}$	–	0.3852	–	0.00123	–	0.2306
$P_{d,z}$	–	0.5926	–	0.02221	–	0.7659

4. Tests in the laboratory and results

4.1. Test at room temperature

The first test was done at room temperature to check if the results were similar to the expected values and if the measurement of the dielectric properties was actually possible with the produced cavity and coupling loops, see Annex A. The empty cavity was connected to a N5245A Agilent PNA, and the resonant frequency of the TE_{011} mode was found to be at $f_0 = 19.422\ GHz$, with an unloaded Q-factor of $Q_0 = 18203$, very close to the simulation results in Tab. 3.2. From Eq. (3.7), with the geometric factor simulated shown in the same table, the surface resistance obtained was $R_S = 36.90\ m\Omega$. This results in a resistivity of copper $\rho = 1.78 \cdot 10^{-8}$, using Eq. (2.12). This value is about 6% higher than the theoretical value used in Sec. 3.3, most probably due to imperfections in the material.

The first dielectric studied was a sample of a single-crystal Rutile. When the sample was added in the resonator with the corresponding PTFE supports, the resonance of the $TE_{01\delta}$ mode was found to be $f_0 = 7.435\ GHz$, and the Q-factor $Q_0 = 9025$. This is by a factor two lower of what we expected. Using the geometric and filling factors mentioned in Tab. 3.3, the loss tangent of PTFE taken from Fig. 4.1 (b), and the surface resistance from the resistivity mentioned above, the resulting loss tangent of Rutile using Eq. (3.1) is $\tan\delta_\perp = 1.117 \cdot 10^{-4}$. Even though this value is twice as high than what is measured in [6], this value is very similar to the one measured in [9], corresponding to a crystal from Alineason [15] from the same batch. Even the crystals from the same batch can differ significantly in their properties and should be measured individually. From the resonant frequency, the relative permittivity was obtained with the aid of CST by matching the resonant frequency of the simulation and measurement, and it resulted to be $\varepsilon_{r,\perp} = 89.92$.

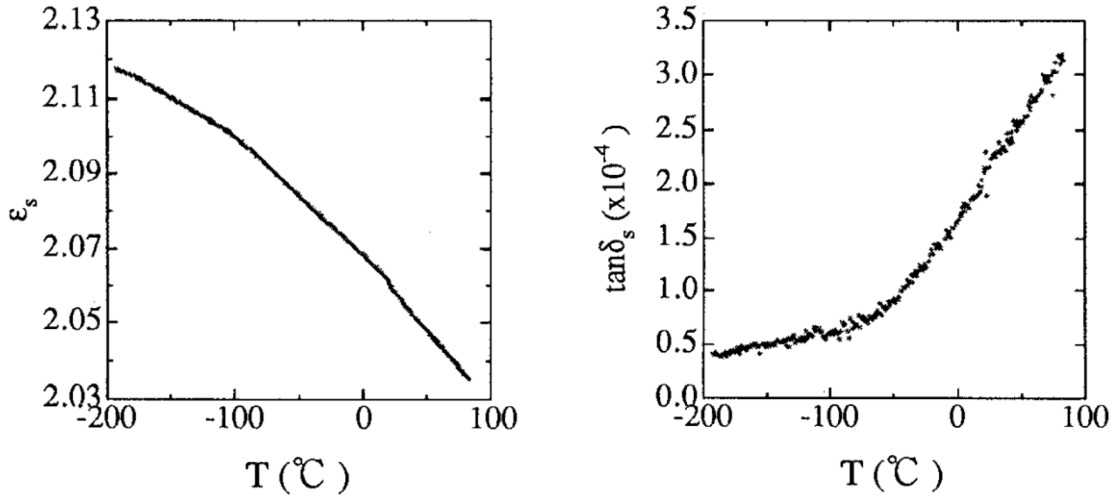

(a) (b)

Figure 4.1: Properties of PTFE in function of temperature (ºC). (a) Relative permittivity. (b) Loss tangent. The measurement was performed at a frequency of 48 GHz [13].

4.2. Measurement procedure

To obtain the dielectric properties as a function of temperature, the resonator was put on top of the cold head of the Janis CCS-250L inside a cryostat, see Fig. 4.2 (a) and (b). Once a satisfactory vacuum was achieved ($\sim 10^{-5}$ mbar) with the help of a compact vacuum system, primary Agilent IDP15 and turbo TwisTorr74FS, the temperature was set to a base value of 25 K. Temperature stabilization was defined by the movement of the resonant frequency peak. If the movement was in the range of kHz, it was considered as stable. Each measurement point was therefore taken after 20 min waiting time.

After the temperature stabilized, the measurements of the centre frequency, loaded quality factor, and the S-Parameters were acquired with the VNA. This process was repeated for small increments of temperature (usually 5 K, 10 K, or 20 K) until room temperature was reached again. After the measurements were done, the data was analyzed and the resonant frequencies and unloaded quality factors were obtained with the aid of a previously developed python based code [16], from which the properties of the dielectric under investigation were calculated in the same way as in Ch. 3, adapting the necessary values.

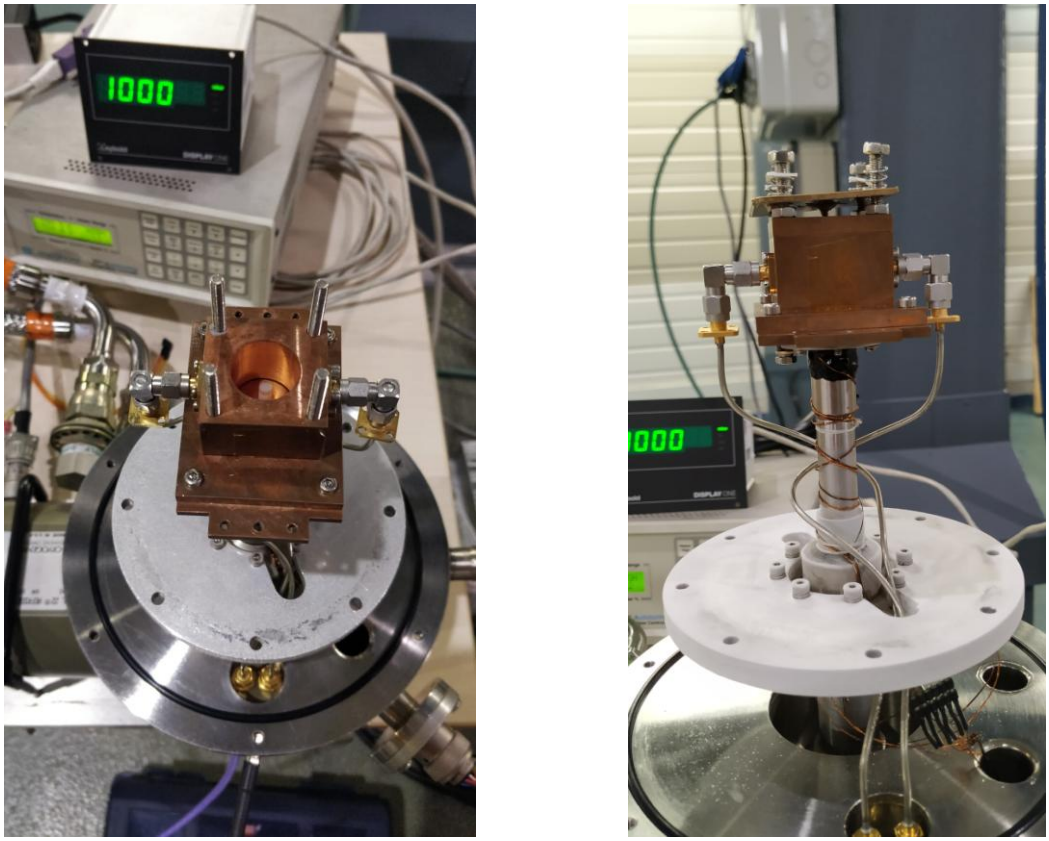

(a) (b)

Figure 4.2: (a) Resonator open from above, mounted on top of the cold plate in the cryogenic refrigerator without radiation shields. The dielectric sample can be seen inside maintained in place by the bottom PTFE support. (b) Closed resonator. The top PTFE support presses the dielectric sample with the help of a plate and four springs.

4.3. Measurement of surface resistance vs. temperature

The temperature dependence of the surface resistance of the copper cavity was measured over the temperature range 25 – 300 K using the TE_{011} mode, see Fig. 4.3. As the temperature varies, the dimensions of the cavity will change according to the thermal expansion coefficient of copper. This is reflected in the resonant frequency in Fig. 4.4. From these parameters, the resistivity of copper shown in Fig. 4.5 for each temperature can be obtained following the same procedure as in Sec. 4.1. It shows the expected linear approximated behavior until low cryogenic temperatures where residual-resistivity can be seen $RRR \approx 6$.

The geometric factor used for the measurements for each temperature is the average value obtained in the simulations at room temperature and 50 K, as it barely changes

and can be considered constant. Therefore, its value is the average between Tab. 3.2 and Tab. 3.4.

To investigate the sensitivity to errors of the measured resistivity, it is necessary to calculate its partial derivatives. From Eqs. (2.12) and (3.7), the resistivity ρ of the copper cavity can be defined as:

$$\rho = \frac{G^2}{f\mu_0\pi Q_0^2} \quad . \tag{4.1}$$

The parameters that contribute to an error are the measured resonant frequency and unloaded Q-factor. Therefore, the partial derivatives needed are the following:

$$\frac{\partial\rho}{\partial f} = -\frac{G^2}{f^2\mu_0\pi Q_0^2} \quad , \tag{4.2}$$

$$\frac{\partial\rho}{\partial Q_0} = -\frac{2G^2}{f\mu_0\pi Q_0^3} \quad . \tag{4.3}$$

Next, to give an estimation of the error in the resistivity ρ, propagation of errors is applied:

$$\Delta\rho = \sqrt{\left(-\frac{G^2\Delta f}{f^2\mu_0\pi Q_0^2}\right)^2 + \left(-\frac{G^2\Delta Q_0}{f\mu_0\pi Q_0^2}\right)^2} = \frac{G^2}{f\mu_0\pi Q_0^2}\sqrt{\left(\frac{\Delta f}{f}\right)^2 + \left(\frac{2\Delta Q_0}{Q_0}\right)^2} \quad . \tag{4.4}$$

The errors were measured based on the average values of two consecutive measurements and the difference between them. At the temperature of 50 K, the measured resonant frequency and quality factor were $f = 19.4874$ GHz and $Q_0 = 41406$, respectively. The resulting errors were $\Delta f = 784$ Hz and $\Delta Q_0 = 40$. After solving Eq. (4.4), the absolute error results in $\Delta\rho = 6.66 \cdot 10^{-12}$ Ωm, and the relative error $\frac{\Delta\rho}{\rho} = 1.95 \cdot 10^{-3}$.

In overall, the errors observed in the resonant frequencies were in the order of 10^4 Hz, and for the unloaded Q-factor in the order of 10^2. The absolute errors in the ρ were in the order of 10^{-11} Ωm, and the relative errors in the order of 10^{-3}. The maximum error measured in the resistivity is of 0.8%.

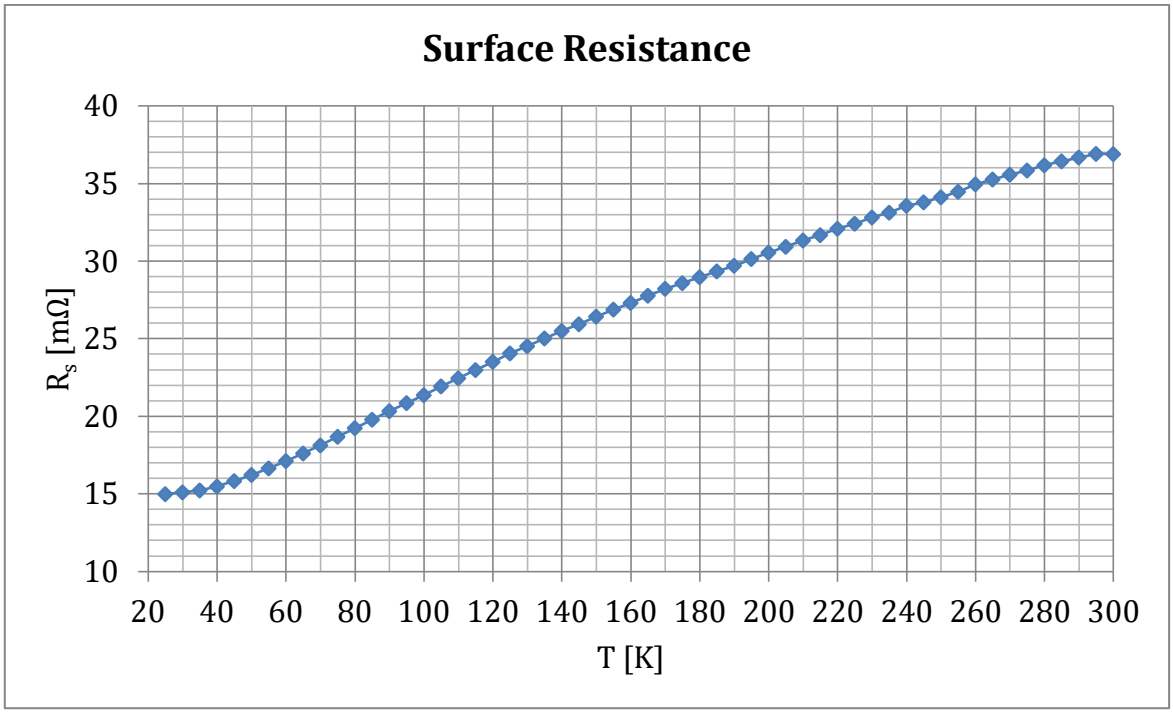

Figure 4.3: Surface resistance R_s of the copper cavity as a function of temperature. The measurement frequency of the TE_{011} mode at room temperature was of 19.422 GHz.

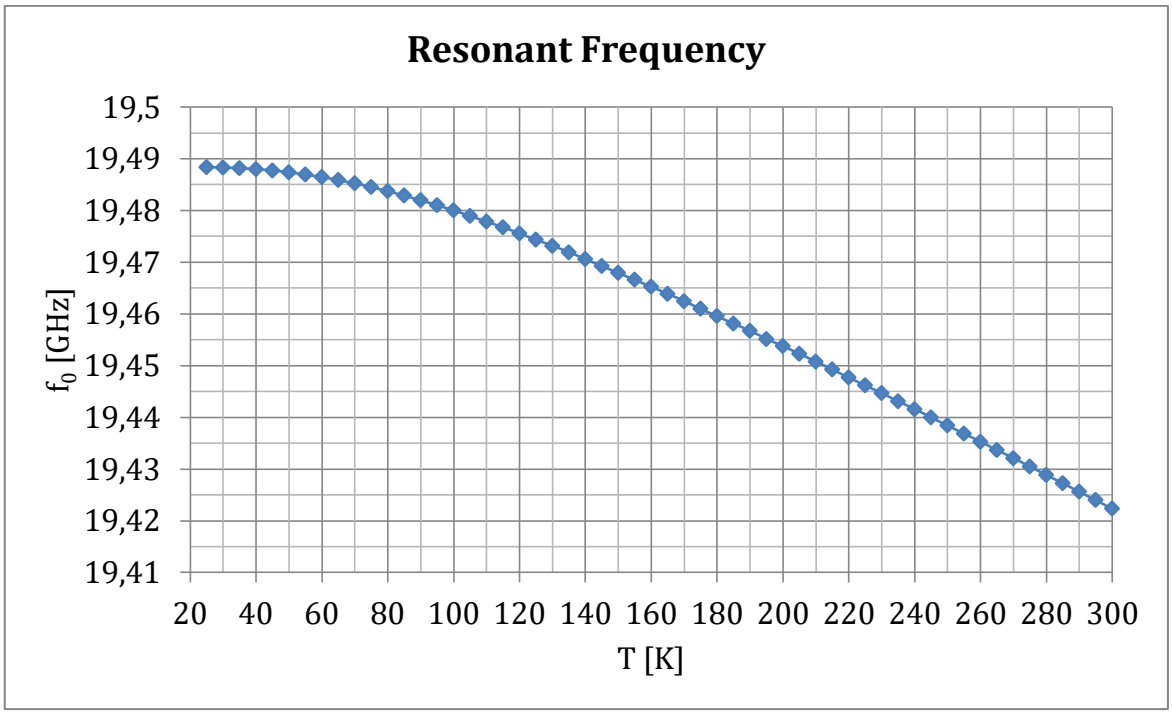

Figure 4.4: Resonant frequency f_0 of copper cavity as a function of temperature.

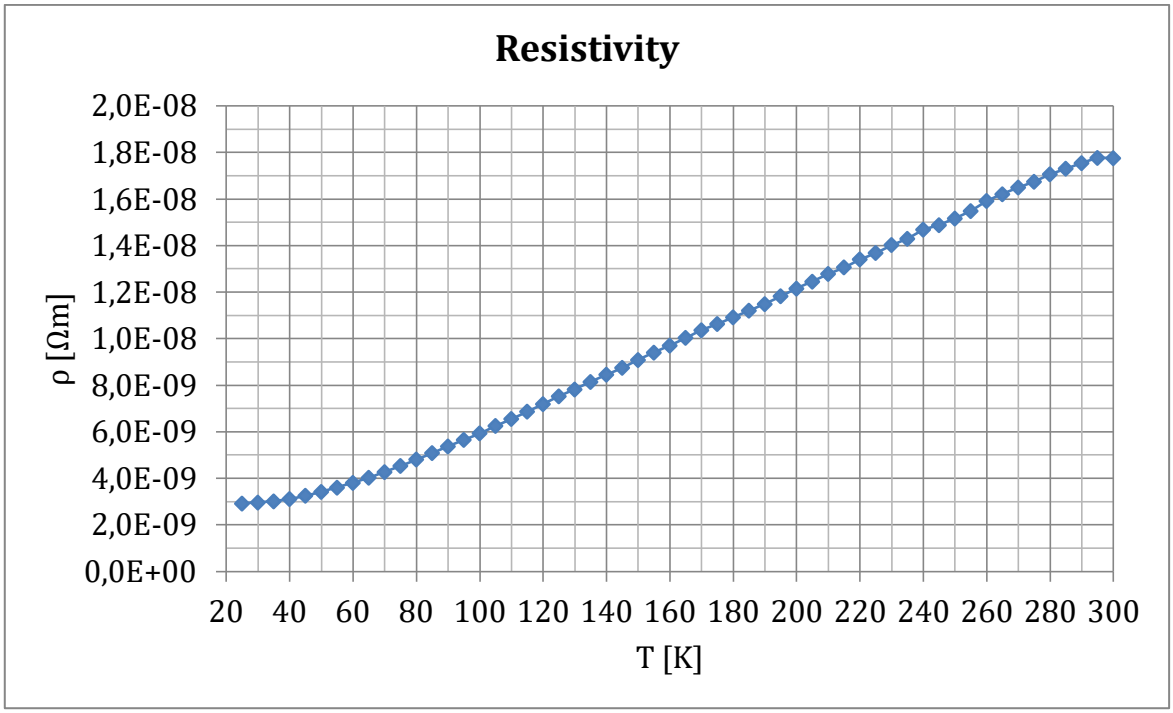

Figure 4.5: Resistivity ρ of the copper cavity as a function of temperature.

4.4. Measurement of Rutile vs. temperature

The dielectric properties of the Rutile sample were obtained for the temperature range 30 – 300 K. In this project, only the TE-mode was tested in the laboratory, so the perpendicular component of the permittivity and loss tangent is obtained. The resonant frequencies obtained for each temperature are shown in Fig. 4.6. They were used to calculate the permittivity as explained in Sec. 4.1, and the results can be seen in Fig. 4.7. It can be seen that the values are comparable to the ones measured in [6] using the PTFE loss tangent and resistivity of copper for each temperature shown in Fig. 4.1 and Fig. 4.5, respectively. Nevertheless, the loss tangent measured (Fig. 4.8) is higher than in [6]. It can be simply explained by the fact that we measured at a much higher resonant frequency. The geometric and filling factors for each temperature will be the average values obtained in the simulations at room temperature and 50 K, as in the previous section. Hence, their values will be the average between Tab. 3.3 and Tab 3.5.

The errors in the calculation of the loss tangent of the Rutile sample can be measured following a similar procedure as the previous section.

The loss tangent can be isolated from Eq. 3.1 as the following:

$$\tan\delta_{\perp} = \frac{1}{P_{d,\phi}}\left(\frac{1}{Q_0} - P_{s,\phi}\tan\delta_{s,\perp} - \frac{R_s}{G}\right) \quad , \tag{4.5}$$

and the partial derivatives of the right-hand side are calculated:

$$\frac{\partial(\tan\delta_{\perp})}{\partial Q_0} = -\frac{1}{P_{d,\phi}Q_0^2} \quad , \tag{4.6}$$

$$\frac{\partial(\tan\delta_{\perp})}{\partial(\tan\delta_s)} = -\frac{P_s}{P_{d,\phi}} \quad , \tag{4.7}$$

$$\frac{\partial(\tan\delta_{\perp})}{\partial R_s} = -\frac{1}{P_{d,\phi}G} \quad , \tag{4.8}$$

from which the estimation of the error in the loss tangent is calculated:

$$\begin{aligned}\Delta(\tan\delta_{\perp}) &= \sqrt{\left(-\frac{\Delta Q_0}{P_{d,\phi}Q_0^2}\right)^2 + \left(-\frac{P_s\Delta(\tan\delta_s)}{P_{d,\phi}}\right)^2 + \left(-\frac{\Delta R_s}{P_{d,\phi}G}\right)^2} \\ &= \frac{1}{P_{d,\phi}}\sqrt{\left(\frac{\Delta Q_0}{Q_0^2}\right)^2 + \left(P_s\Delta(\tan\delta_s)\right)^2 + \left(\frac{\Delta R_s}{G}\right)^2} \quad .\end{aligned} \tag{4.9}$$

The error in the surface resistance ΔR_s is obtained from the measured unloaded quality factor of the empty cavity, as it works at a higher frequency and will be a worst-case scenario, besides easing the calculations. From Eq. (3.7), the surface resistance can be isolated:

$$R_s = \frac{G}{Q_0} \quad , \tag{4.10}$$

and its partial derivatives are calculated:

$$\frac{\partial R_s}{\partial Q_0} = -\frac{G}{Q_0^2} \quad . \tag{4.11}$$

As a result, we obtain the following estimation of the error in the surface resistance:

$$\Delta R_s = \sqrt{\left(-\frac{G\Delta Q_0}{Q_0^2}\right)^2} = \frac{G\Delta Q_0}{Q_0^2} \quad . \tag{4.12}$$

The errors in this case were also based in the average between two different measurements and their difference. At 50 K, the error in the surface resistance obtained from the empty cavity measurements and using Eq. (4.12) is of $\Delta R_s = 1.58 \cdot 10^{-5}\ \Omega$. For the cavity filled with the Rutile sample, the measured quality factor was of $Q_0 = 200426$, and the error was of $\Delta Q_0 = 685$. The error in the PTFE loss tangent is obtained from [13], with a value of $\Delta(\tan\delta_s) = 2 \cdot 10^{-5}$. Then,

from Eq. (4.9) we obtain an absolute error of $\Delta(\tan\delta_\perp) = 3.94 \cdot 10^{-8}$, and a relative error of $\frac{\Delta(\tan\delta_\perp)}{\tan\delta_\perp} = 8.53 \cdot 10^{-3}$.

The errors measured in the surface resistance are in the order of 10^{-4} Ω. For the cavity filled with the Rutile sample, the measurement errors of the quality factor are in the order of 10^2. The absolute errors in the $\tan\delta_\perp$ are then in the order of 10^{-7}, and the relative errors in the order of 10^{-2}. The maximum value obtained for the measured error in the loss tangent is of 1.2%.

The error in the permittivity was measured by performing a number of tests at room temperature, where the dielectric sample was removed and put again, and observing the differences in the measured resonant frequencies. From these values, the variation in the permittivity was obtained from simulations in CST. The relative error calculated from five different measurements was of $\frac{\Delta\varepsilon}{\varepsilon} = 3.024 \cdot 10^{-3}$, which in the Rutile sample corresponds to a maximum absolute error of $\Delta\varepsilon = 0.35$.

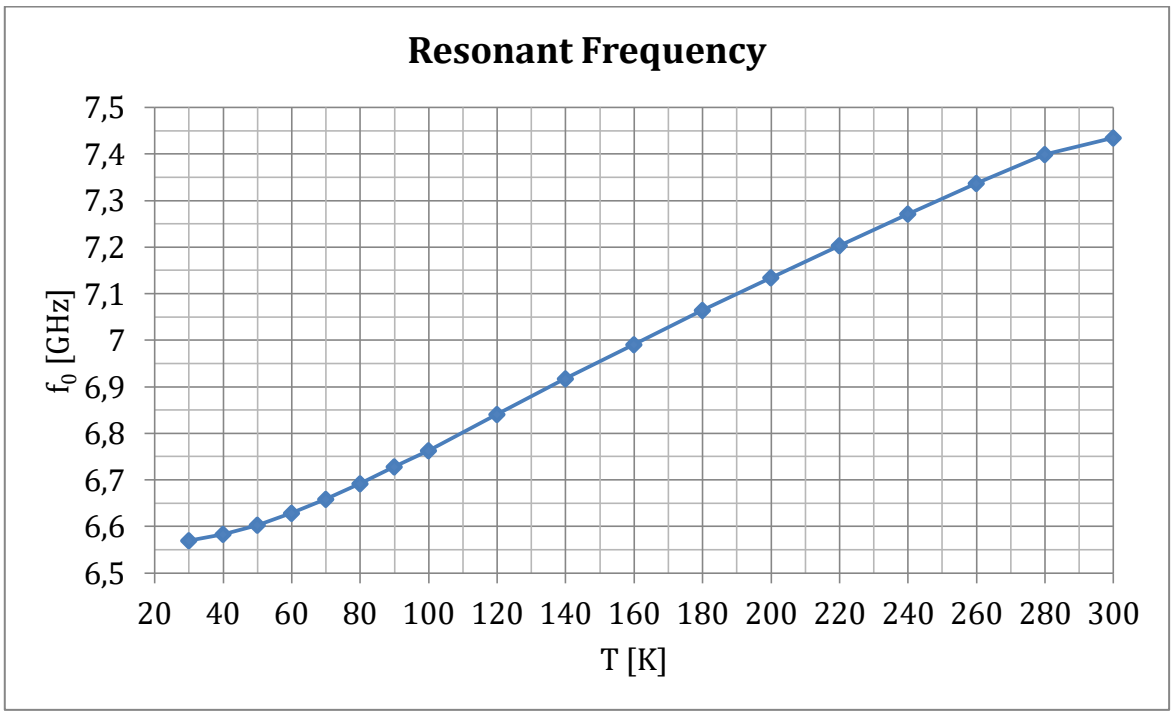

Figure 4.6: Measured resonant frequencies of the $TE_{01\delta}$ mode for the resonator filled with Rutile as a function of temperature.

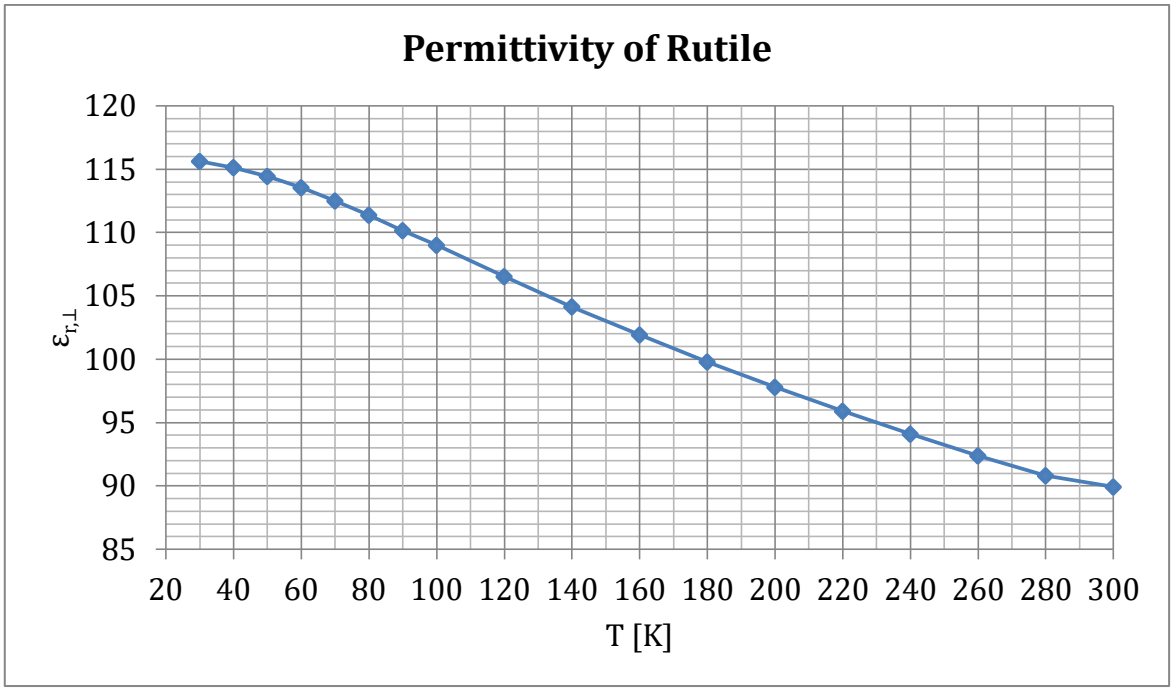

Figure 4.7: Perpendicular component of the relative permittivity of Rutile (TiO_2) as a function of temperature. The measurement frequency of the $TE_{01\delta}$ mode at room temperature was 7.435 GHz.

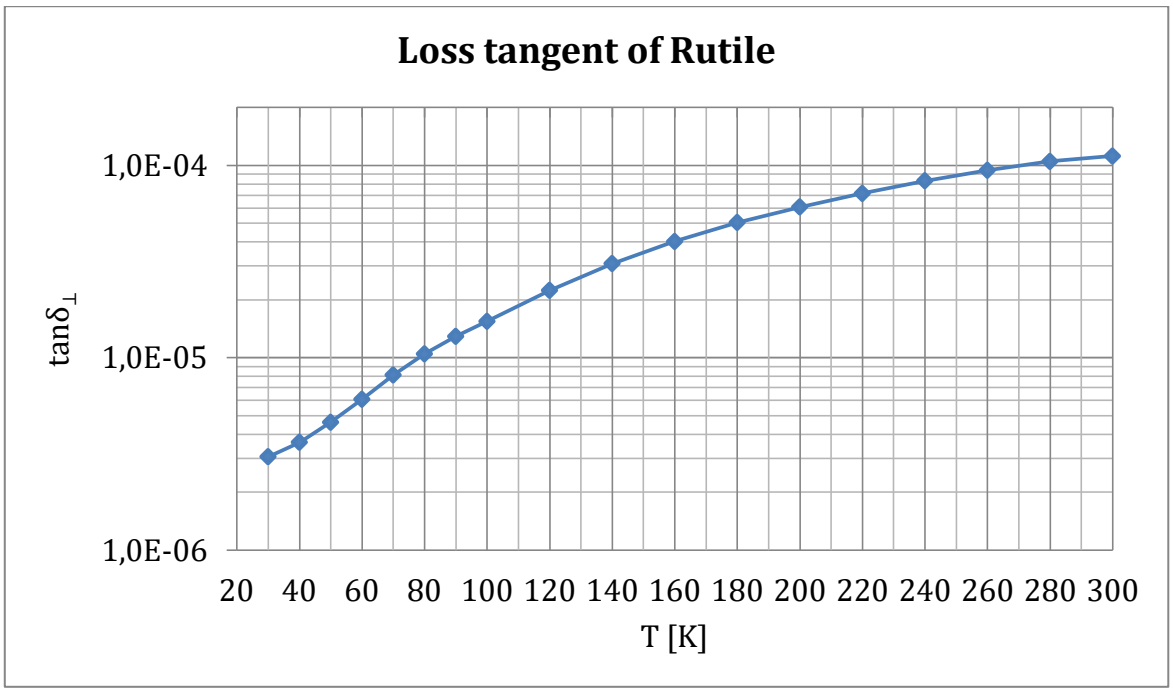

Figure 4.8: Perpendicular component of the loss tangent (log scale) of Rutile (TiO_2) as a function of temperature. The measurement frequency of the $TE_{01\delta}$ mode at room temperature was 7.435 GHz.

4.5. Measurement of Strontium Titanate vs. temperature

Single-crystal Strontium Titanate is an interesting dielectric material due to its high permittivity at low temperatures. A sample of this dielectric was tested with the resonator to measure its properties over a range of temperature of 30 – 100 K. In this case, the geometric and filling factors had to be simulated for each temperature individually, since the permittivity of this dielectric changes greatly as it approaches cryogenic temperatures. Hence, the geometric and filling factors changed considerably and they could no longer be assumed constant. The resonant frequency values for each temperature are shown in Fig. 4.9, from which the permittivity in function of temperature is simulated, see Fig. 4.10. The obtained loss tangent in the range of temperature can be seen in Fig. 4.11. The results obtained in a frequency range of 1.2 - 2 GHz are in the same magnitude to the ones measured in Fig. 4.12 [14], where lower frequencies were used. The frequency dependence of the loss tangent is not clear in the figure. It also shows how at below 80 K the loss tangent of this dielectric changes his behavior and its value starts increasing, same as in our case.

The errors in the measurement of the Strontium Titanate sample can be measured the same way and with the same equations as in the previous section. Therefore, the errors in the surface resistance and loss tangent of PTFE have the same values. In this case, the errors were obtained from five different measurements and their average values. At a temperature of 50 K, the error for the Q-factor was $\Delta Q_0 = 99.37$ and the Q-factor of $Q_0 = 4571$. This results from Eq. (4.9) in an absolute error in the loss tangent of $\Delta(\tan\delta_\perp) = 4.76 \cdot 10^{-6}$, and a relative error of $\frac{\Delta(\tan\delta_\perp)}{\tan\delta_\perp} = 2.18 \cdot 10^{-2}$.

From the overall, the errors in the measured quality factor are in the order of tens. The absolute errors are in the order of 10^{-6} , and the relative errors in the order of 10^{-2}. The maximum error observed in the loss tangent is of 2.2%.

The error in the permittivity is measured the same way as in the previous section, which results to an absolute error between $\Delta\varepsilon = 14.70$ and $\Delta\varepsilon = 3.81$, for 30 and 100 K, respectively.

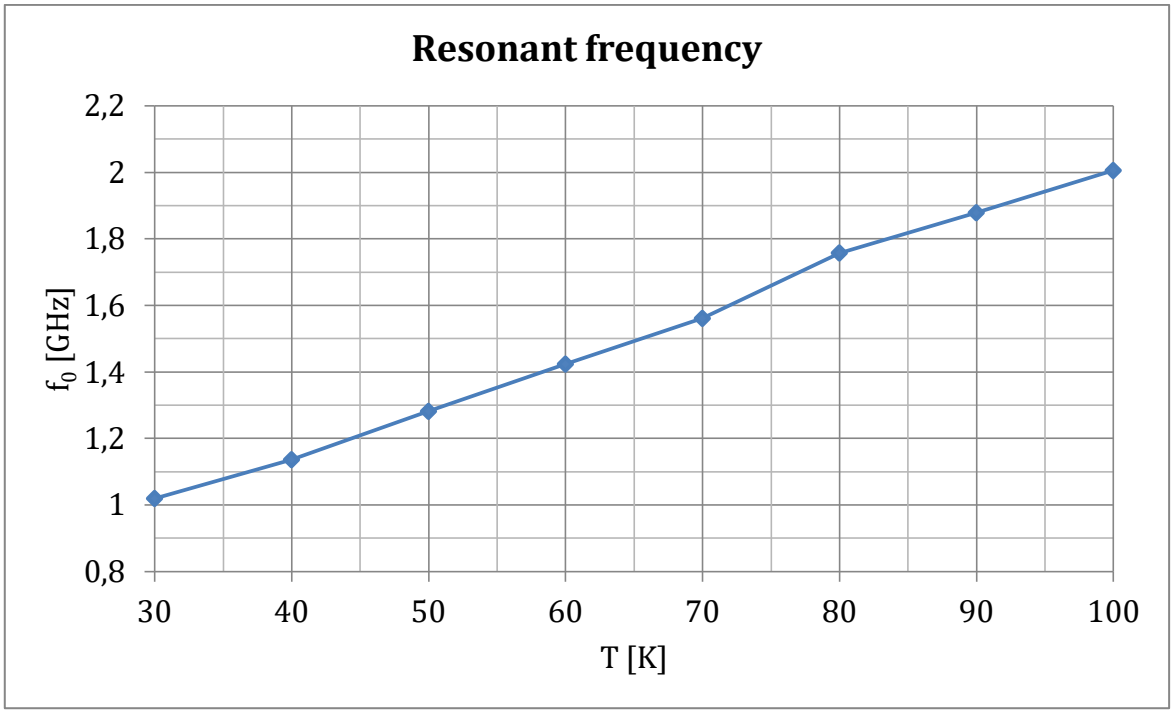

Figure 4.9: Measured resonant frequencies of the $TE_{01\delta}$ mode for the resonator filled with Strontium Titanate as a function of temperature.

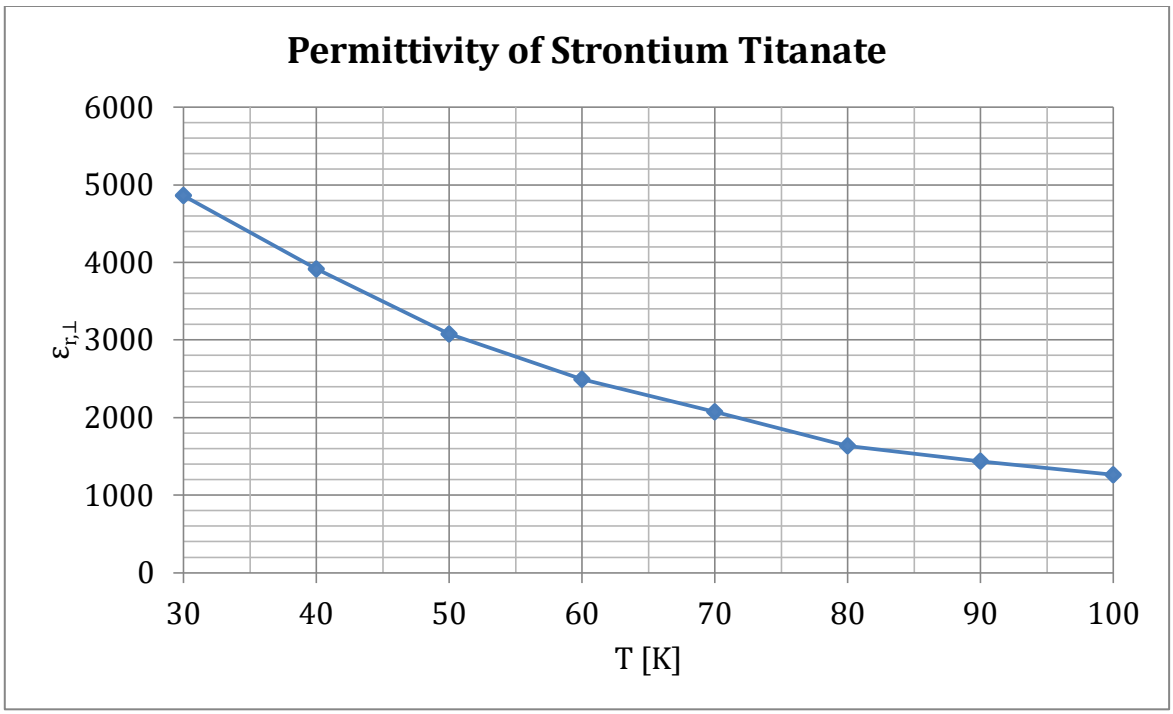

Figure 4.10: Perpendicular component of the relative permittivity of Strontium Titanate ($SrTiO_3$) as a function of temperature. The measurement frequency of the $TE_{01\delta}$ mode at 50 K was 1.282 GHz.

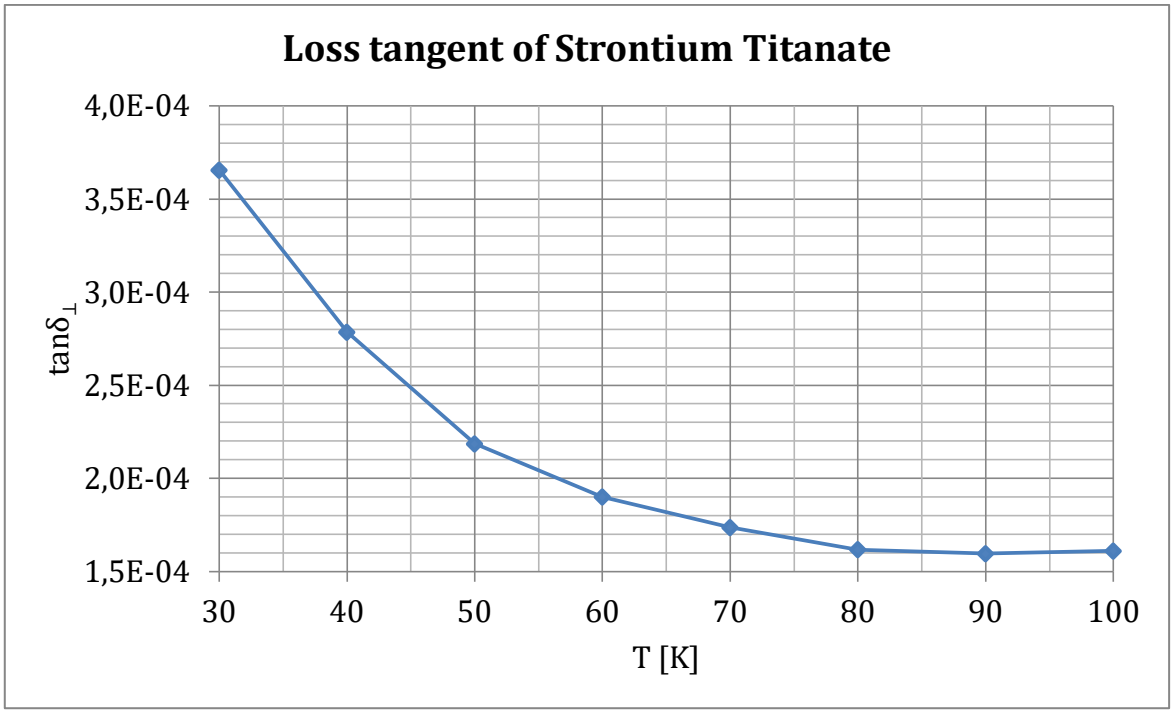

Figure 4.11: Perpendicular component of the loss tangent (log scale) of Strontium Titanate ($SrTiO_3$) as a function of temperature. The measurement frequency of the $TE_{01\delta}$ mode at 50 K was 1.282 GHz.

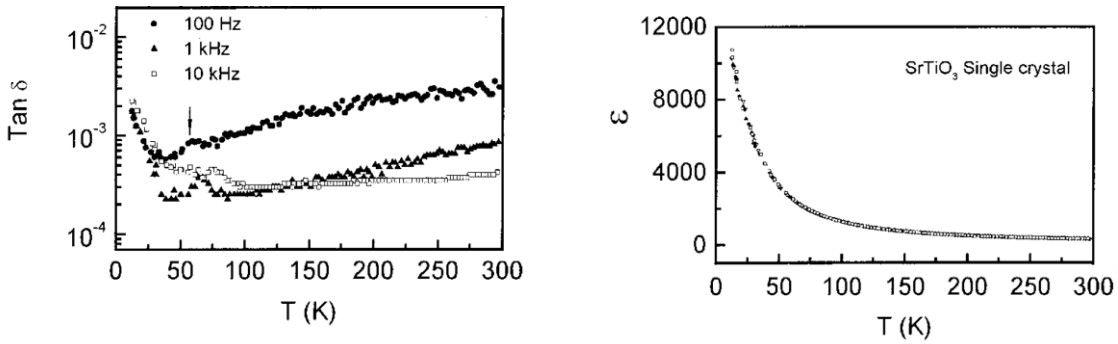

(a) (b)

Figure 4.12: Temperature dependence of loss tangent (a) and permittivity (b) as function of frequencies for a Strontium Titanate single-crystal. Figures taken from [14].

5. Budget

The materials needed for the construction of the resonator had a total cost of around 150€, mainly because of the copper.

The license of the CST software costs 10000€ per year. This software has been used practically during this entire project, which lasted around 7 months.

The engineering student has dedicated 30 hours per week during 28 weeks, which is a total of 840 hours. The degree tutor has collaborated with 1 hour meeting every week, plus the time dedicated in literature review, revisions, and mail correspondences. These hours can be assumed on an average of 5 hours per week, during 28 weeks. Therefore, the tutor has devoted a total of 140 hours.

The salaries corresponding to these jobs can be characterized in the following way:

- The Junior Engineer has a gross salary of 9 €/h. Including the social charges, results in a total cost of 12 €/h.
- The cost of the Degree Thesis Tutor is of approximately 30 €/h, including the social security.

Finally, the Budget for this project is the following:

Concept	Quantity	Cost	Total cost
Resonator materials	1	150 €	150 €
CST license	7 months	10000 €/year	5833 €
Junior Engineer	840 h	12 €/h	10080 €
Degree thesis tutor	140 h	30 €/h	4200 €

6. Summary, conclusions and outlook

This project aimed to design a resonator capable of measuring the permittivity and loss tangent properties of different dielectric samples. A series of CST simulations has been done to determine the dimensions of the resonator suited for this purpose.

Once the resonator was build, we were able to measure the properties of interest for Rutile and Strontium Titanate samples, but was not suited for the Sapphire sample, due to its very low loss tangent, causing a low sensitivity in the measurements. Anyway, Sapphire loss tangent is so low that we can measure the R_s of the HTS-CCs with good accuracy without having a precise knowledge of its loss tangent. The results were compared to other matching studies, and the similarities found demonstrated a high level of confidence.

A study of the errors concluded that the measured loss tangent has a relative error of 1.2% for the Rutile sample and 2.2% for the Strontium Titanate. For the permittivity, the absolute error is higher the higher the permittivity of the dielectric under study, nevertheless, they were calculated to be less than 1%.

From this study, the data obtained for Rutile can be used for the measurement of the surface impedance of the HTS-CCs proposed as coating for the FCC at CERN. The loss tangent of Strontium Titanate, as being one magnitude higher, has to be proven experimentally if it is still low enough to measure R_s accurately.

For future improvements, a repetition of the measurements would be desirable to confirm the values, as well as to give robustness to the results. To measure the properties of Sapphire for the TE-mode, the diameter of the actual resonator can be enlarged. Also, a better support material like a single-crystal Quartz could be used. Further, to reduce the surface losses of the walls the cavity could be coated with silver, which would help to measure the parallel components of the microwave properties. To add the parallel component of the permittivity and loss tangent, the TM-mode discussed in this project should be investigated further, especially

electrical contacts between closing plates of the cavity. A better system to maintain the crystal in place and capable of resisting vibrations could also be improved. Finally, a full automation of the process could be made to speed up the measurements.

Appendices A:

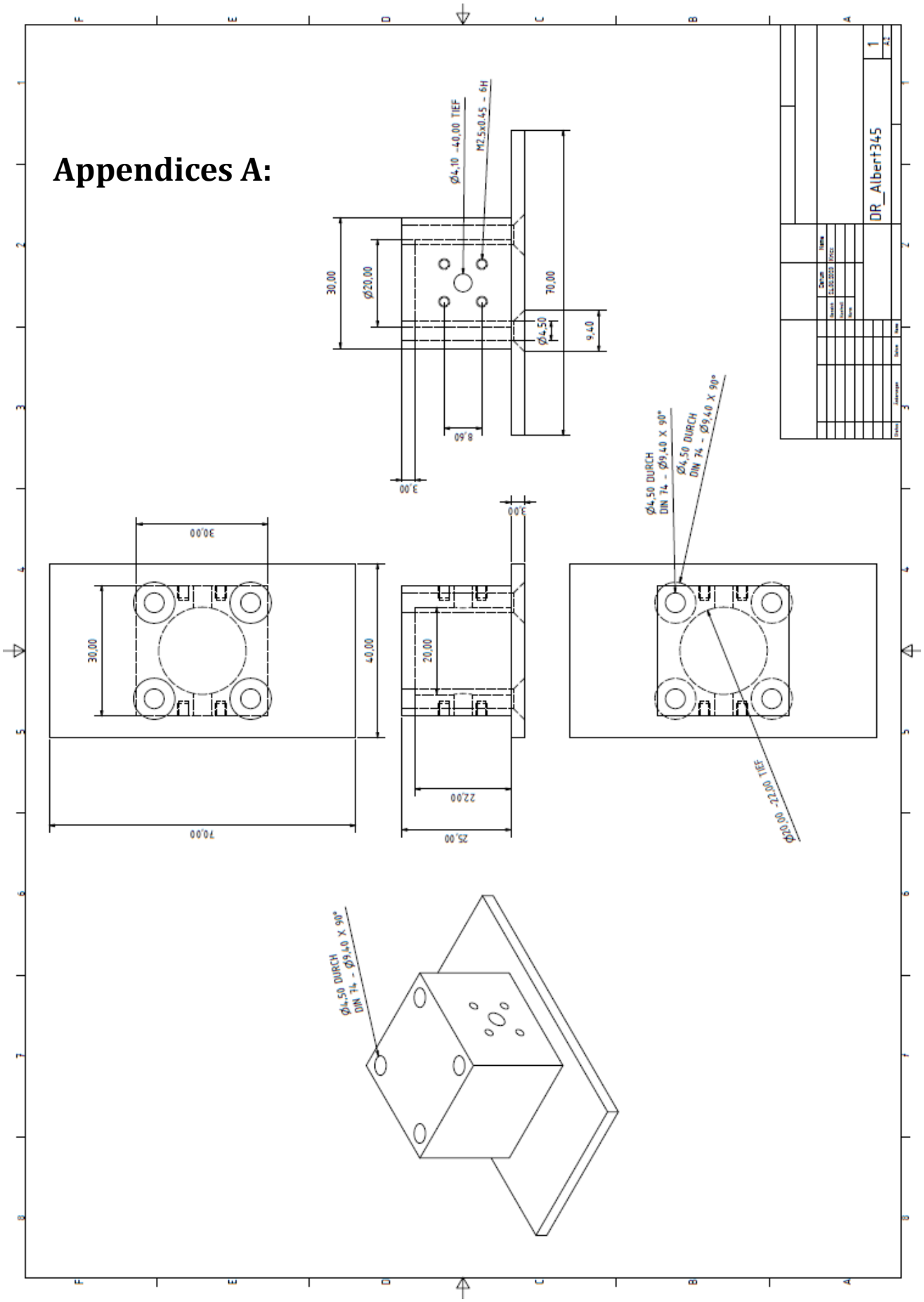

Glossary

ALBA	ALBA Synchroton
CCs	Coated Conductors
CERN	Conseil Européen pour la Recherche Nucléaire
CST	Computer Simulation Technology
DUT	Device under test
FCC	Future Circular Collider
HTS	High-temperature superconductors
ICMAB	Institut de Ciència de Materials de Barcelona
IFAE	Institut de Física d'Altes Energies
LHC	Large Hadron Collider
PEC	Perfect Electric Conductor
PTFE	Polytetrafluoroethylene
RRR	Residual-resistivity ratio
UPC	Universitat Politècnica de Catalunya
VNA	Vector Network Analyzer

Bibliography:

[1] CERN Future Circular Collider website. Available at: https://fcc-cdr.web.cern.ch/

[2] Future Circular Collider Study. Volume 1: Physics Opportunities. Conceptual Design Report, preprint edited by M. Mangano et al. CERN accelerator reports, CERN-ACC-2018-0056, Geneva, December 2018. Published in Eur. Phys. J. C

[3] Future Circular Collider Study. Volume 2: The Lepton Collider (FCC-ee) Conceptual Design Report, preprint edited by M. Benedikt et al. CERN accelerator reports, CERN-ACC-2018-0057, Geneva, December 2018. Published in Eur. Phys. J. ST.

[4] Future Circular Collider Study. Volume 3: The Hadron Collider (FCC-hh) Conceptual Design Report, preprint edited by M. Benedikt et al. CERN accelerator reports, CERN-ACC-2018-0058, Geneva, December 2018. Published in Eur. Phys. J. ST.

[5] Future Circular Collider Study. Volume 4: The High Energy LHC (HE-LHC) Conceptual Design Report, preprint edited by F. Zimmermann et al. CERN accelerator reports, CERN-ACC-2018-0059, Geneva, December 2018. Published in Eur. Phys. J. ST.

[6] J. Breeze, "Temperature and Frequency Dependence of Complex Permittivity in Metal Oxide Dielectrics: Theory, Modelling and Measurement", Springer Theses, Springer International Publishing AG 2016, DOI: 10.1007/978-3-319-44547-2_3

[7] CST Studio Suite®. Simulation software of electromagnetic fields. Available at: https://www.3ds.com/es/productos-y-servicios/simulia/productos/cst-studio-suite/

[8] D.M. Pozar. *Microwave Engineering*. 4th ed. John Wiley and Sons, Inc, 2011.

[9] P. Krkotić, A. Aguasca and J. M. O'Callaghan, "Small Footprint Evaluation of Metal Coatings for Additive Manufacturing," *2018 48th European Microwave Conference (EuMC)*, Madrid, 2018, pp. 882-885, doi: 10.23919/EuMC.2018.8541442.

[10] P. Krkotić. Private communication.

[11] N. Klein et al. *Dielectric properties of rutile and its use in high temperature superconducting resonators*. AIP Journal of Applied Physics, Vol. 78, No. 11, 1 December 1995.

[12] M.V. Jacob, J.Mazierska, K.Leong, J.Krupka. *Microwave properties of low-loss polymers at cryogenic temperatures*. IEEE transactions on microwave theory and techniques, Vol. 50, No. 2, February 2002.

[13] G. Zhang, S. Nakaoka and Y. Kobayashi. "Millimeter wave measurements of temperature dependence of complex permittivity of dielectric plates by the cavity resonance method". Department of Electrical and Electronic Engineering, Saitama University, 255 shimo-okubo, Urawa, Saitama 338 Japan.

[14] C. Ang, R. Guo, A.S. Bhalla, L.E. Cross. *Effect of electric field and post-treatment on dielectric behavior of $SrTiO_3$ single crystal*. AIP Journal of Applied Physics, Vol. 87, No. 8, 15 April 2000. Materials Research Laboratory, The Pennsylvania State University, University Park.

[15] Alineason website. Available at: https://www.alineason.com/

[16] Patrick Krkotić, Queralt Gallardo, Nikki Tagdulang, Montse Pont, and Joan M. O'Callaghan. Novel Algorithm for Resonator Parameter Extraction with Outlier Removal. Submitted to IEEE Transactions on Microwave Theory and Techniques. September 2020.